# Comparison of Roadway Roughness Derived from LIDAR and SFM 3D Point Clouds

OCTOBER 2015

## Final Report

CENTER FOR
CEER
EARTHWORKS ENGINEERING
RESEARCH


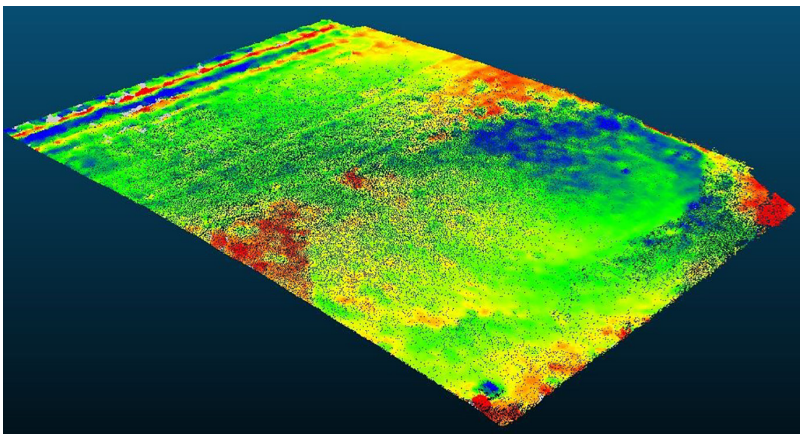

IOWA STATE UNIVERSITY
Institute for Transportation

**Sponsored by**
Iowa Department of Transportation
(HR-3001 InTrans Project 15-543)

## About the Center for Earthworks Engineering Research

The mission of the Center for Earthworks Engineering Research (CEER) at Iowa State University is to be the nation's premier institution for developing fundamental knowledge of earth mechanics, and creating innovative technologies, sensors, and systems to enable rapid, high quality, environmentally friendly, and economical construction of roadways, aviation runways, railroad embankments, dams, structural foundations, fortifications constructed from earth materials, and related geotechnical applications.

## Disclaimer Notice

The contents of this report reflect the views of the authors, who are responsible for the facts and the accuracy of the information presented herein. The opinions, findings and conclusions expressed in this publication are those of the authors and not necessarily those of the sponsors.

The sponsors assume no liability for the contents or use of the information contained in this document. This report does not constitute a standard, specification, or regulation.

The sponsors do not endorse products or manufacturers. Trademarks or manufacturers' names appear in this report only because they are considered essential to the objective of the document.

## ISU Non-Discrimination Statement

Iowa State University does not discriminate on the basis of race, color, age, ethnicity, religion, national origin, pregnancy, sexual orientation, gender identity, genetic information, sex, marital status, disability, or status as a U.S. veteran. Inquiries regarding non-discrimination policies may be directed to Office of Equal Opportunity, Title IX/ADA Coordinator, and Affirmative Action Officer, 3350 Beardshear Hall, Ames, Iowa 50011, 515-294-7612, email eooffice@iastate.edu.

## Iowa Department of Transportation Statements

Federal and state laws prohibit employment and/or public accommodation discrimination on the basis of age, color, creed, disability, gender identity, national origin, pregnancy, race, religion, sex, sexual orientation or veteran's status. If you believe you have been discriminated against, please contact the Iowa Civil Rights Commission at 800-457-4416 or the Iowa Department of Transportation affirmative action officer. If you need accommodations because of a disability to access the Iowa Department of Transportation's services, contact the agency's affirmative action officer at 800-262-0003.

The preparation of this report was financed in part through funds provided by the Iowa Department of Transportation through its "Second Revised Agreement for the Management of Research Conducted by Iowa State University for the Iowa Department of Transportation" and its amendments.

The opinions, findings, and conclusions expressed in this publication are those of the authors and not necessarily those of the Iowa Department of Transportation.

**Technical Report Documentation Page**

| 1. Report No. | 2. Government Accession No. | 3. Recipient's Catalog No. |
|---|---|---|
| InTrans Project 15-543 | | |

| 4. Title and Subtitle | 5. Report Date |
|---|---|
| Comparison of Roadway Roughness Derived from LIDAR and SFM 3D Point Clouds | October 2015 |
| | **6. Performing Organization Code** |

| 7. Author(s) | 8. Performing Organization Report No. |
|---|---|
| Ahmad Alhasan, Kyle Younkin, and David J. White | InTrans Project 15-543 |

| 9. Performing Organization Name and Address | 10. Work Unit No. (TRAIS) |
|---|---|
| Center for Earthworks Engineering and Research<br>Iowa State University<br>2711 South Loop Drive, Suite 4700<br>Ames, IA 50010-8664 | **11. Contract or Grant No.** |

| 12. Sponsoring Organization Name and Address | 13. Type of Report and Period Covered |
|---|---|
| Iowa Department of Transportation | Final Report |
| 800 Lincoln Way<br>Ames, IA 50010 | **14. Sponsoring Agency Code**<br>Iowa DOT Project HR-3001 |

**15. Supplementary Notes**

Visit www.intrans.iastate.edu and www.ceer.iastate.edu for color pdfs of this and other research reports.

**16. Abstract**

This report describes a short-term study undertaken to investigate the potential for using dense three-dimensional (3D) point clouds generated from light detection and ranging (LIDAR) and photogrammetry to assess roadway roughness. Spatially continuous roughness maps have potential for the identification of localized roughness features, which would be a significant improvement over traditional profiling methods. This report specifically illustrates the use of terrestrial laser scanning (TLS) and photogrammetry using a process known as structure from motion (SFM) to acquire point clouds and illustrates the use of these point clouds in evaluating road roughness. Five roadway sections were chosen for scanning and testing: three gravel road sections, one portland cement concrete (PCC) section, and one asphalt concrete (AC) section. To compare clouds obtained from terrestrial laser scanning and photogrammetry, the coordinates of the clouds for the same section on the same date were matched using open source computer code. The research indicates that the technologies described are very promising for evaluating road roughness. The major advantage of both technologies is the large amount of data collected, which allows the evaluation of the full surface. Additional research is needed to further develop the use of dense 3D point clouds for roadway assessment.

| 17. Key Words | 18. Distribution Statement |
|---|---|
| 3D point clouds—laser scan—LIDAR—pavement performance—pavement roughness—photogrammetry—road smoothness—structure from motion—surface characteristics—terrestrial scan | No restrictions. |

| 19. Security Classification (of this report) | 20. Security Classification (of this page) | 21. No. of Pages | 22. Price |
|---|---|---|---|
| Unclassified. | Unclassified. | 60 | NA |

**Form DOT F 1700.7 (8-72)** **Reproduction of completed page authorized**

# COMPARISON OF ROADWAY ROUGHNESS DERIVED FROM LIDAR AND SFM 3D POINT CLOUDS

**Final Report**
**October 2015**

**Principal Investigator**
David J. White, Director
Center for Earthworks Engineering and Research, Iowa State University

**Research Assistants**
Ahmad Alhasan and Kyle Younkin

**Authors**
Ahmad Alhasan, Kyle Younkin, and David J. White

Sponsored by
the Iowa Department of Transportation
(Iowa DOT Project HR-3001)

Preparation of this report was financed in part
through funds provided by the Iowa Department of Transportation
through its Research Management Agreement with the
Institute for Transportation
(InTrans Project 15-543)

A report from
**Center for Earthworks Engineering and Research**
**Institute for Transportation**
**Iowa State University**
2711 South Loop Drive, Suite 4700
Ames, IA 50010-8664
Phone: 515-294-8103 / Fax: 515-294-0467
www.ceer.iastate.edu

## TABLE OF CONTENTS

## LIST OF FIGURES

## LIST OF TABLES

## ACKNOWLEDGMENTS

The authors would like to thank the Iowa Department of Transportation (DOT) for sponsoring this research and Story and Boone Counties in Iowa for access to their projects.

## EXECUTIVE SUMMARY

This report describes a short-term study undertaken to investigate the potential for using dense three-dimensional (3D) point clouds generated from light detection and ranging (LIDAR) and photogrammetry to assess roadway roughness. Spatially continuous roughness maps have potential for the identification of localized roughness features, which would be a significant improvement over traditional profiling methods. Few studies have illustrated the procedure to obtain roughness maps, and there are no standardized procedures to develop and analyze features in these maps. This report specifically illustrates the use of terrestrial laser scanning (TLS) and photogrammetry using a process known as structure from motion (SFM) to acquire point clouds and illustrates the use of these point clouds in evaluating road roughness.

Two technologies were chosen to acquire 3D point clouds of the road sections under consideration: (a) stationary or terrestrial 3D laser scanning and (b) photogrammetry. LIDAR systems measure information (spatial coordinates and color) of a 3D space and stores the information in a 3D point cloud. Photogrammetry involves interpreting photographic images and patterns of electromagnetic radiant energy. Modern photogrammetry has been revolutionized by the process of SFM.

In this study, five sections were chosen for scanning and testing: three gravel road sections, one portland cement concrete (PCC) section, and one asphalt concrete (AC) section. After cleaning and segmenting the point clouds, the data were processed using algorithms developed to produce roughness maps. The first step in analyzing the data was to form a mesh grid from the discrete measurement points. Evaluation of roughness in this study is based on the responses of a mechanical system that would approximate the response of a passenger vehicle (quarter-car model per ASTM E1926-08 [2008]). To compare clouds obtained from terrestrial laser scanning and photogrammetry, the coordinates of the clouds for the same section on the same date were matched using open source computer code.

To analyze the spatial difference in elevation between the clouds acquired from terrestrial laser scanning and photogrammetry, the point clouds resulting from both methods were compared. It was determined that in most cases the highest difference is at rough locations. This might be due to the limitation of the laser scanner in capturing points covered by other features in the view or due to the fact that the photogrammetry algorithm produces high noise around these features due to the shadows and different lightning conditions at such features. To confirm these hypotheses, further testing is needed.

In brief, the study at hand presented the tools to evaluate road roughness of different road types using 3D point clouds collected using two different technologies: terrestrial laser scanning and photogrammetry. The research indicates that the technologies described are very promising for evaluating road roughness. The major advantage of both technologies is the large amount of data collected, which allows the evaluation of the full surface. Additional research is needed to further develop the use of dense 3D point clouds for roadway assessment.

# CHAPTER 1: INTRODUCTION

Surface roughness maps offer continuous roughness measurements along the road length and across its width, allowing identification of localized rough features. This is a significant improvement over some traditional roughness evaluation procedures that involve profiling one or a few lines across the road width, especially for applications involving automated machine guidance (AMG). With the recent developments in data acquisition systems, such as light detection and ranging (LIDAR) and photogrammetry, several profiler manufacturers have developed technologies capable of acquiring coincident multi-profiles to produce an approximation of surface roughness maps.

To date, the results from research and demonstration projects have shown promise in using continuous roughness maps in the evaluation of road roughness and in localized feature detection to optimize maintenance activities and real-time quality control/assurance (QC/QA). However, results are limited. Few studies have illustrated the procedure to obtain roughness maps. Based on the literature review conducted for this research, there are no studies comparing the use of different technologies for collecting input data for these maps, and there are no studies utilizing these maps to study the development of rough features over time and the correlation between the roughness of consecutive layers in a pavement system. Finally, there are no standardized procedures to develop these maps and analyze the rough features and the information contained in them. This report illustrates the use of terrestrial laser scanning (TLS) and photogrammetry to acquire point clouds and illustrates the use of these point clouds in evaluating road roughness.

## CHAPTER 2: OVERVIEW OF ROUGHNESS EVALUATION TECHNIQUES

Pavement roughness has been a major pavement performance indicator since the early twentieth century (Buchanan et al. 1941, Nakamura 1962). Gillespie et al. (1980) described methods to quantify pavement roughness using time-stable calibrated response-type systems. After 1986, the international roughness index (IRI) was established as a standard pavement roughness measurement (Sayers et al. 1986a, Sayers et al., 1986b). IRI and other roughness indices are summary statistics, and since their development the main focus has been on increasing the accuracy of measurement and the repeatability of results. However, there is little agreement on how to quantify local feature roughness, even though studies have shown that local features are crucial to human comfort and cause most vehicle fatigue damage (Steinwolf et al. 2002, Oijer and Edlund 2004, Bogsjö and Rychlik 2009).

As defined by Sayers and Karamihas (1998), "a profiler is an instrument used to produce a series of numbers related in a well-defined way to a true profile." Measuring devices fall into two categories: systems that measure the coordinates of points along a linear track (geometry-type systems) and systems that measure the response of mechanical systems driven along a track (response-type road roughness measure [RTRRM] systems).

One of the basic geometry-type systems is the static-level system. In this method, the elevations of sampled points along a line are recorded. The true elevation of a point is not critical; rather, the change in elevation relative to a reference point is the main concern (Gillespie et al. 1987). This technique is physically demanding and time consuming, yet it is stable and reliable. ASTM E1364–95 is the standard method to perform static-level measurements.

Other geometry-type systems are available, including dipstick, rolling dipstick, rolling straightedge, and Hearne straightedge (El-Korchi and Collura 1998, El-Korchi et al. 2002, Perera and Kohn 2002), but all of these devices are relatively time consuming compared to inertial profilers. Inertial profilers were developed in the 1960s (Spangler and Kelly 1964) and were standardized in ASTM E950. These profilers are more accurate and faster than other profilers, hence the name high-speed profilers (Choubane et al. 2002).

High-speed profilers consist of four main components: an accelerometer, one or more non-contact height sensor(s), a speedometer, and a computer. The accelerometer measures the vertical acceleration of the height sensor. The height sensor(s) records the elevation from the ground using a laser or infrared or ultrasonic waves. The longitudinal distance relative to a reference point is measured by processing the speedometer readings. The computer processes the acceleration data to construct an inertial reference to filter out the height sensor's motion due to suspension. Finally, the computer combines these inputs and produces a sequence of distance versus elevation readings (Baus and Hong 2004).

Researchers have addressed the need to investigate new techniques in profiling using different scanning technologies. Some of these studies have focused on modifications to inertial profilers to involve a broader variety of sensors, such as non-contact wide-footprint and multi-point height sensors (Fernando and Walker 2013, Fernando et al. 2014). Chang and Chang (2006)

investigated the applicability of using stationary three-dimensional (3D) laser scanning techniques in obtaining IRI values.

In the last decade, many construction projects have utilized emerging technologies such as building information model (Chau et al. 2004, Suermann 2009) and intelligent compaction (White et al. 2007). While these are specific technologies, the term automated machine guidance (AMG) is generic and includes monitoring and controlling the construction process using near real-time measurements and feedback loops that can react to the encountered conditions (Hannon 2007, Barrett 2008, White and Vennapusa 2009). Several successful projects have utilized AMG. Anderegg and Kaufmann (2004) reported that intelligent compaction can help optimize compaction and prove the homogeneity and the achieved degree of compaction.

Rasmussen et al. (2013) reported several real-time smoothness measuring systems. Among these systems is the GOMACO smoothness indicator (GSI), which includes up to eight traces, two sonic sensors, and a slope sensor on each trace. Another system is the real-time profiler by Ames Engineering. Multiple systems can be installed across a lane to collect data along more than one trace. Both systems have real-time graphics displays and calculate IRI and profile index (PI), and both have a bump alarm that warns of localized features.

## CHAPTER 3: DATA COLLECTION METHODS

Two technologies were chosen to acquire 3D point clouds of the road sections under consideration: (a) stationary or terrestrial 3D laser scanning (LIDAR) and (b) photogrammetry. Both technologies produce 3D point clouds, where each point has x, y, and z coordinates, and thus both technologies can provide measurements in a 3D space. Descriptions of both technologies and the procedures followed in collecting data are provided below.

### Data Collection Using Stationary Laser Scanner

LIDAR systems measure the information (spatial coordinates and color) of a 3D space and store the information in a 3D point cloud. The term LIDAR is generic and includes airborne laser scanning technologies, mobile scanners mounted on vehicles, and stationary laser scanners or stationary terrestrial laser scanners, where the laser scanner is fixed at a station with known coordinates and a geospatially referenced 3D point cloud is constructed based on the distance between the scanner and the detected points. The Trimble CX 3D stationary terrestrial laser scanning system was used in this study to acquire 3D laser scans. The positional accuracy of a single point is 4.5 mm at 30 m and drops to 7.3 mm at 50 m. The distance accuracy is 1.2 mm at 30 m and drops to 2 mm at 50 m. Figure 1 shows the scanner setup.


**Figure 1. Trimble CX 3D laser scanner setup**

The scanning process starts by acquiring a full scan that covers the 360° by 300° view. This scan produces a mother file that includes common targets (Figure 2) to be used for registration in post-processing.

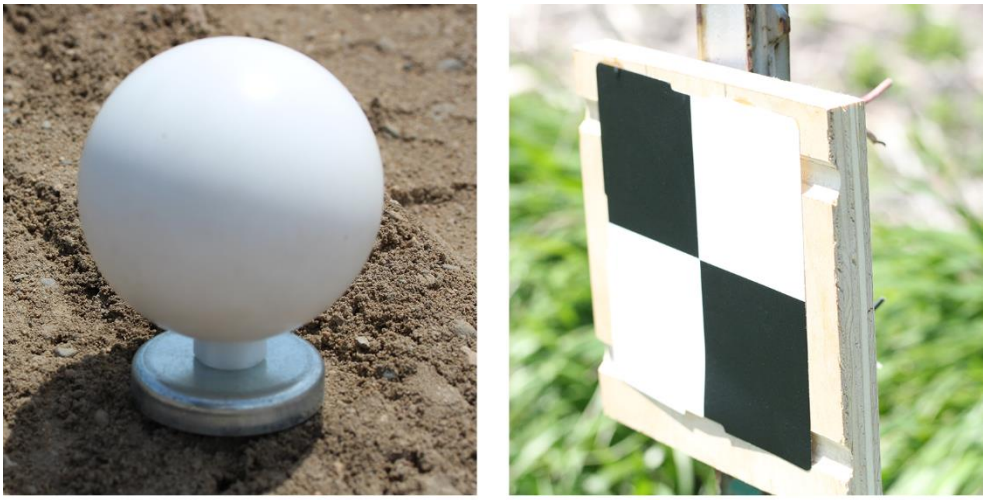


**Figure 2. Reference points for scanning: (a) a spherical target and (b) a flat black and white target**

Three flat targets were attached to fence posts. Each post was driven and fixed to identify a station's region. Area scans were then conducted to acquire denser point clouds for the areas of interest. The size of the targets affect the density of the full scan; smaller targets require high-density full scans to capture. However, the density of the area scans can vary depending on the application. In the two case studies, the criterion specified to analyze road roughness from the point cloud was a maximum spacing of 100 mm at 100,000 mm in both spatial directions (longitudinal and transverse) between two consecutive points. From several trials it was found that a density of 35 mm at 100,000 mm for the area scans produced sufficiently dense clouds to satisfy the 100 mm spacing criterion.

After acquiring the data, the scan is registered in specialized software. Many activities, such as registration and fitting of geometries, can be performed using software packages. Point clouds are registered by identifying common targets (spheres or flat targets, as shown in Figure 2) appearing in the full scans that share a common spatial domain with other scans taken at a different time or at different stations. These targets are used as benchmarks to geospatially reference scans by matching the common target locations in each scan and thus stitching the scans together to produce a full 3D cloud. Figure 3 shows an example of a registered point cloud. The variation in color indicates the material's reflectivity.

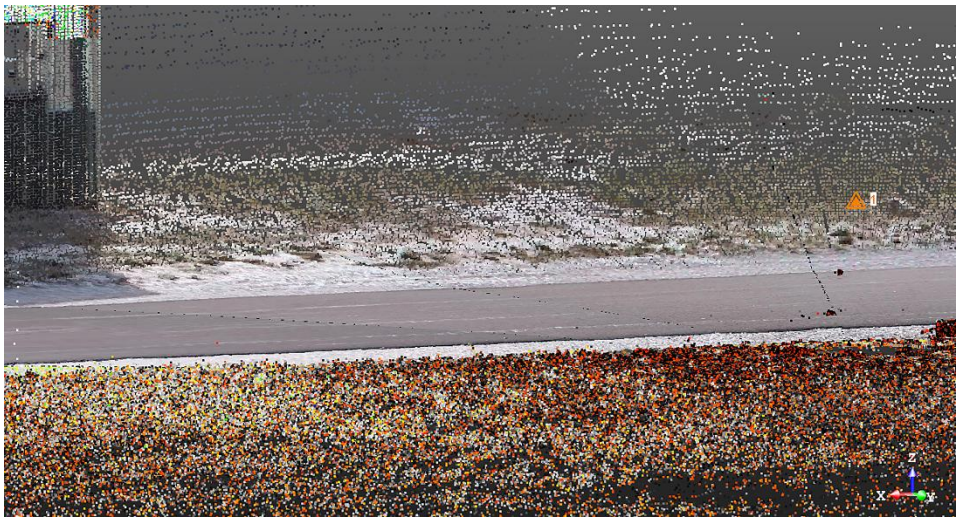

**Figure 3. Registered point cloud of a new asphalt pavement surface**

After registration, the point clouds are cleaned of unnecessary data points: the sections of interest are separated from areas beyond the edges of the sections and from noise from any passing vehicles that might appear in the scans. The final data points left after cleaning can be exported in ASCII file format or any other suitable file format; these files contain the x, y, and z coordinates of the points in the section under consideration.

## Data Collection Using Photogrammetry

Photogrammetry is defined as "the art, science, and technology of obtaining reliable information about physical objects and the environment through processes of recording, measuring, and interpreting photographic images and patterns of electromagnetic radiant energy and other phenomena" (Slama 1980). Modern photogrammetry has been revolutionized by the process known as structure from motion (SFM). This term refers to the process in which the simultaneous position of the camera (motion) and the positions of feature objects (structure) are estimated by analyzing a series of photographs (Snavely 2010). This automated process has made photogrammetry a revolutionary tool that the engineering and geoinformatic communities have been exploring extensively for the last decade (Westoby 2012).

Photographs were taken on a Nikon D90 SLR with an 18–133 mm lens set at 18 mm for the widest field of view. The aperture was generally set at f/13 in order to increase the depth of focus, and if sunlight was sufficient the shutter speed was set at around 1/200 seconds to give better clarity while taking moving shots. In general, the camera resolution should be no lower than 2,500 pixels; higher resolution images will reduce processing time but increase point density. The optimum time for image capture is within two to three hours during midday to reduce shadow zones that can diminish the accuracy of the model. The section to be compared was traversed around the perimeter with pictures taken every one to two seconds to provide 90% overlap between images for better key point recognition. However, some software like Agisoft PhotoScan only requires 75% overlap. Several 5 and 40 m sections were captured on county

highways in rural Story and Boone Counties in Iowa. Images were collected within an hour of the laser scan being taken. The number of images varied by length of roadway.

In the first step of SFM computation, the process of scale-invariant feature transform (SIFT) is used on the photographs (Lowe 2004). SIFTing utilizes extrema detection to extract unique key points from photographs using a difference-of-Gaussian function (Figure 4).

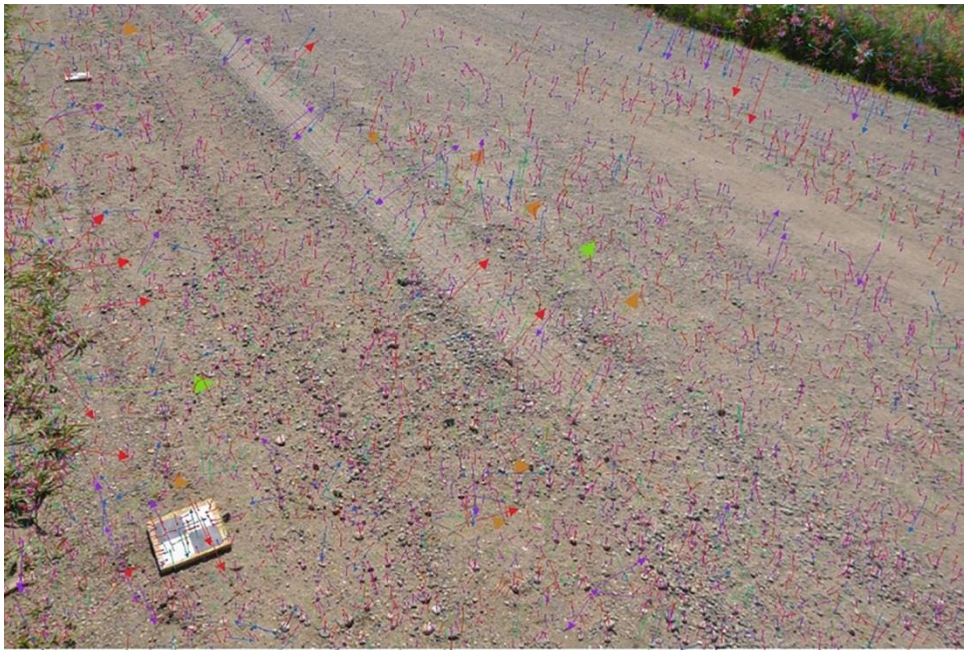

**Figure 4. SFM key point recognition using a difference-of-Gaussian function (see colored arrows)**

After features are recognized and matched, they are reconstructed from key points (Figure 5).

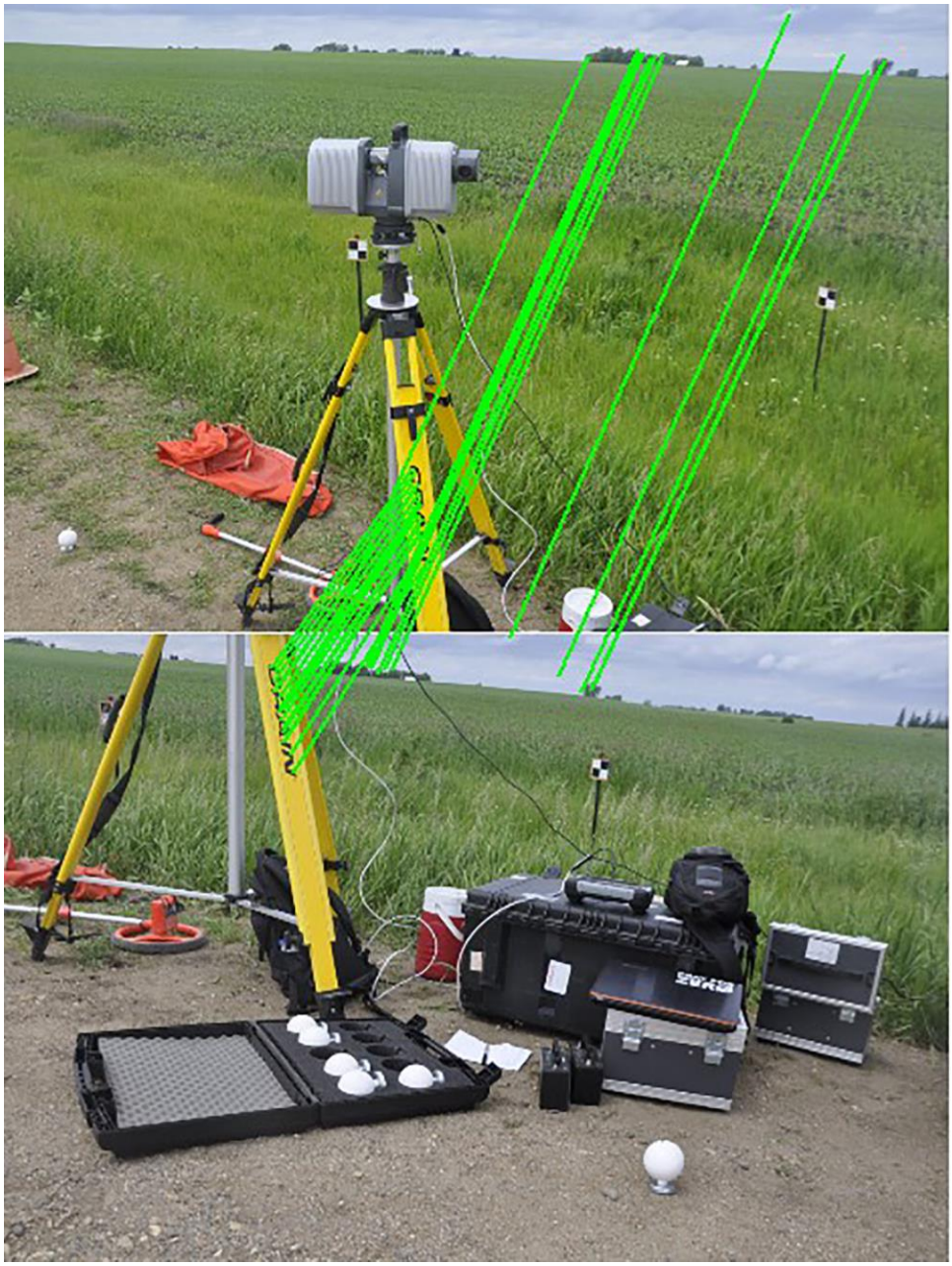

**Figure 5. Key point matching inliers between two overlapping images (green lines)**

As mentioned above, SFM is the process of simultaneously estimating both geometry (structure) and camera position and angle (motion). This process is automated in the graphical user interface package called VisualSFM (Wu 2013). Once the sparse reconstruction is finished, more points can be computed using external algorithms that have been integrated into VisualSFM. There are several available packages, but VisualSFM includes clustering views for multi-view stereo (CMVS) and patch-based multi-view stereo (PMVS).

VisualSFM breaks down the images into sets of 50 and creates a denser point cloud using the output from the previous step (Figure 6).

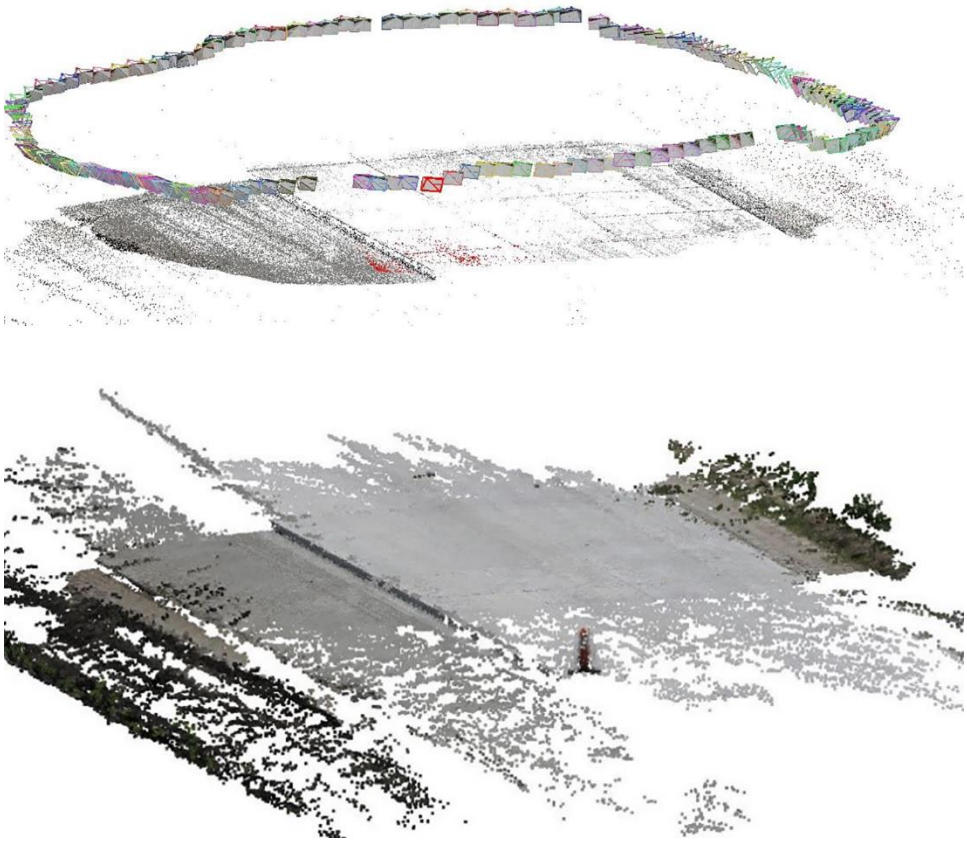

**Figure 6. SFM reconstruction showing estimated camera positions (top) and dense reconstruction using CMVS (bottom)**

Multiple programs and feature matching settings were tested, each of which took anywhere from 45 minutes for a series of 30 images to 30 hours for 450 images on a standard desktop computer with an 8 GB RAM Quad Core processor without a dedicated CPU. This is a CPU-intensive process that requires robust hardware. New SFM software tends to utilize cloud-based reconstruction that only requires the uploading of image sets to a server and downloading of the point cloud or mesh (Autodesk 2015).

## Alternative Georeferencing Tools

In addition to the traditional flat and spherical targets provided by the manufacturer, a 76.2 mm diameter spherical target, shown in Figure 7, was designed and printed at the Iowa State University College of Design for $40. The cost of Trimble targets previously purchased was more than $100 per sphere.

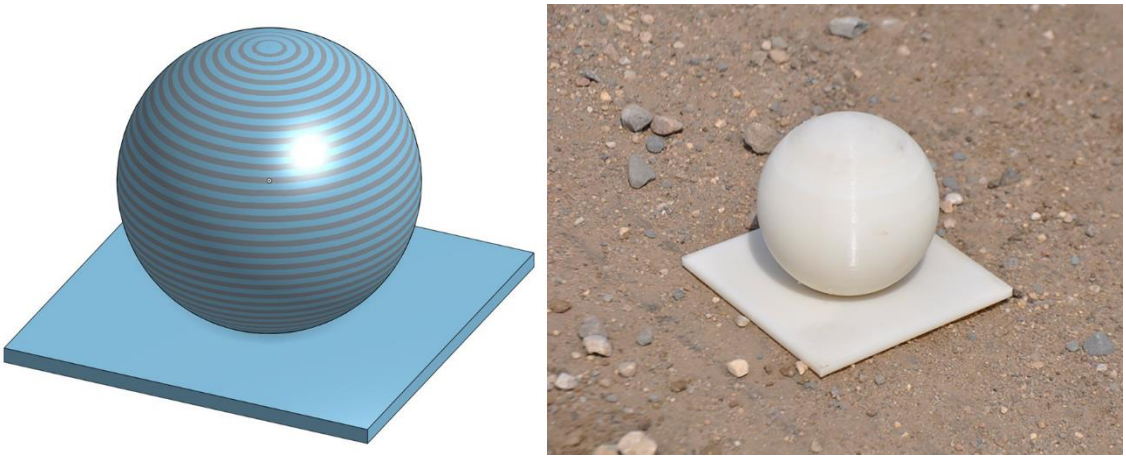

**Figure 7. 3D model of spherical target (left) and printed speherical target (right)**

Table 1 shows the root mean square (RMS) values resulting from fitting a spherical surface to the points acquired from both a Trimble target and the 3D-printed target.

**Table 1. Fitting errors of spherical targets**

| Scan | Trimble Target 1 RMS (mm) | 3D-Printed Target RMS (mm) |
|---|---|---|
| 10 m | 0.87 | 1.27 |
| 5 m | 1.22 | 0.76 |
| 10 m | 1.17 | 1.32 |
| 5 m | 1.14 | 1.24 |

Four scans were acquired at 10 m and 5 m from the target. It can be seen in Table 1 that the RMS values for both spheres were close, indicating that printed spheres can be considered as a cheaper alternative than the manufacturer's target. However, further investigation is needed to evaluate the printed spheres' performance under various conditions.

### 3D-Printed Roadway

Another product of the study that serves as a visual aid was a 3D-printed model of a roadway. The 3D print was for a corrugated gravel section with evident rutting. The point cloud collected via photogrammetry was used to construct a mesh utilizing a Poisson algorithm in Blender software (Figure 8).

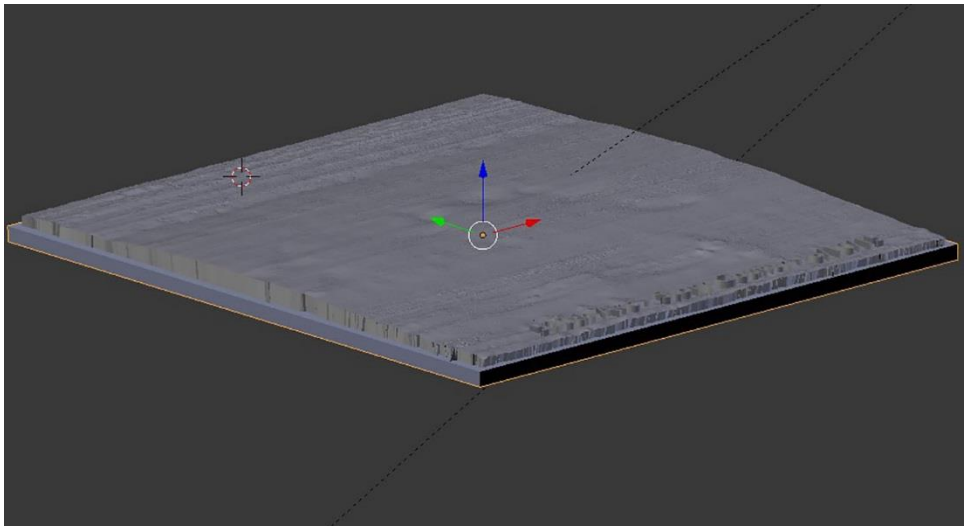

**Figure 8. 3D model of gravel road developed in Blender (v 2.76)**

This 3D mesh is a collection of triangles defined by three points and a normal surface vector. The 3D mesh was then exported to Blender, an open source 3D modeling software package, to solidify the surface mesh, attach the base, and add letters. The model was scaled to a 1/50 ratio, and measurements were taken of crown height, rut size, and lane width.

3D-printed road surfaces can be useful in visualization and educational purposes. Initially, the model was printed on a Stratasys Mojo printer with a 170 μm (0.00669 in.) resolution (Figure 9).

**Figure 9. 3D-printed model of gravel road from a low-resolution Stratasys Mojo printer**

However, most of the road surface features were lost due to the low resolution of the print. The model was then printed on a Stratasys Polyjet printer with VeroBlue material at a 30 µm (0.00118 in.) resolution (Figure 10).

**Figure 10. High-resolution 3D-printed model of a gravel road from a Stratasys Polyjet printer**

With this high-resolution print, even small surface variations were captured. These models could be used in variety of presentations and workshops on deteriorating unpaved roads across Iowa.

## CHAPTER 4: TEST SECTIONS AND EXPERIMENTAL TEST RESULTS

Five sections were chosen for scanning and testing: three gravel sections, one portland cement concrete (PCC) section, and one asphalt concrete (AC) section. Samples were collected from the gravel sections when possible to conduct sieve analyses. However, no samples were collected for the Story County section because the surface consisted of a large-size crushed limestone layer over a stiff crust. Dynamic cone penetration (DCP) tests were conducted at three test points (TPs) for each lane. Based on the data collected and using the DCP index (DCPI), defined as the amount of penetration divided by the number of blows causing the penetration, California bearing ratios (CBR) were estimated using equations (1), (2), and (3):

for CBR>10, DCP-CBR = $292/(\text{DCPI} \times 25.4)^{1.12}$ **(1)**
for CBR>10, DCP-CBR = $292/(\text{DCPI} \times 25.4)^{1.12}$ **(2)**
for CBR>10, DCP-CBR = $292/(\text{DCPI} \times 25.4)^{1.12}$ **(3)**

### Boone County Sections

*West Section*

This section is located on 210th Street in rural Boone County. County employees noted that the road has an unusually high amount of traffic for an unpaved road. Traffic included a mix of cars, trucks, and semi-trailers. There is constant traffic 600 m (2,000 ft) from the closest intersection. The north side of the road was blocked off for an hour during scan days. The approximate coordinates of the laser scanner station were 42°2’57.31”N, 93°45’52.69”W. Figure 11 shows the section on different days and in different conditions.

**Figure 11. West section of 210th Street at different times: May 28 (left), June 3 (middle), and June 4 (right); blading occurred before May 28 and after June 4**

Figure 12 shows the gradation curve of the surface materials collected from the site on May 28. The samples were collected at two locations. It can be seen in Figure 12 that there is no evidence for a large variation in the material gradation. However, further testing is needed to verify this observation.

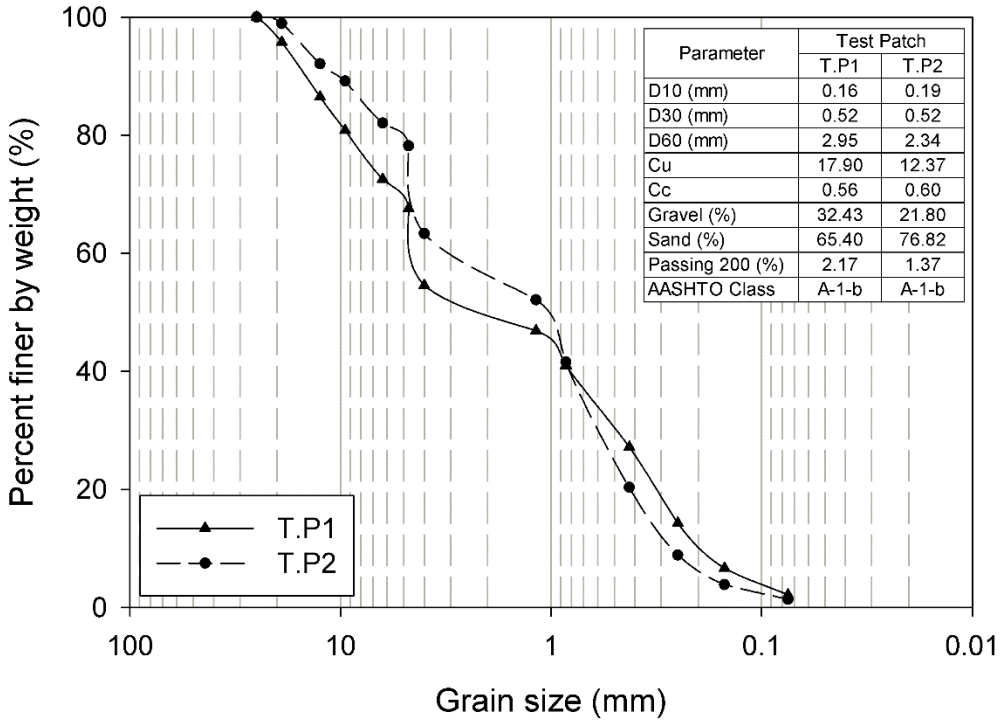


**Figure 12. Grain size distribution of surface material for west section of 210th Street in Boone County, Iowa**

Figure 13 (a) and Figure 13 (b) show DCPI versus depth for the three test points tested on May 22 in the right lane heading east and in the left lane heading west, respectively. Figure 13 (c) and Figure 13 (d) show DCP-CBR versus depth for the same three test points.

Tests were conducted to an approximate depth of 50 cm. It can be seen in Figure 13 that there are stiff laminae (DCP-CBR > 80%) down to depths of 15 cm. However, the top 5 cm are weaker, which corresponds to the loose materials at the surface. Figure 14 shows the results for approximately the same test points tested on May 25. Very similar trends were observed on both dates. However, the soils became weaker over time for the first 20 cm. Refusals were observed at TP 2 at 16 cm on May 22 and May 25.

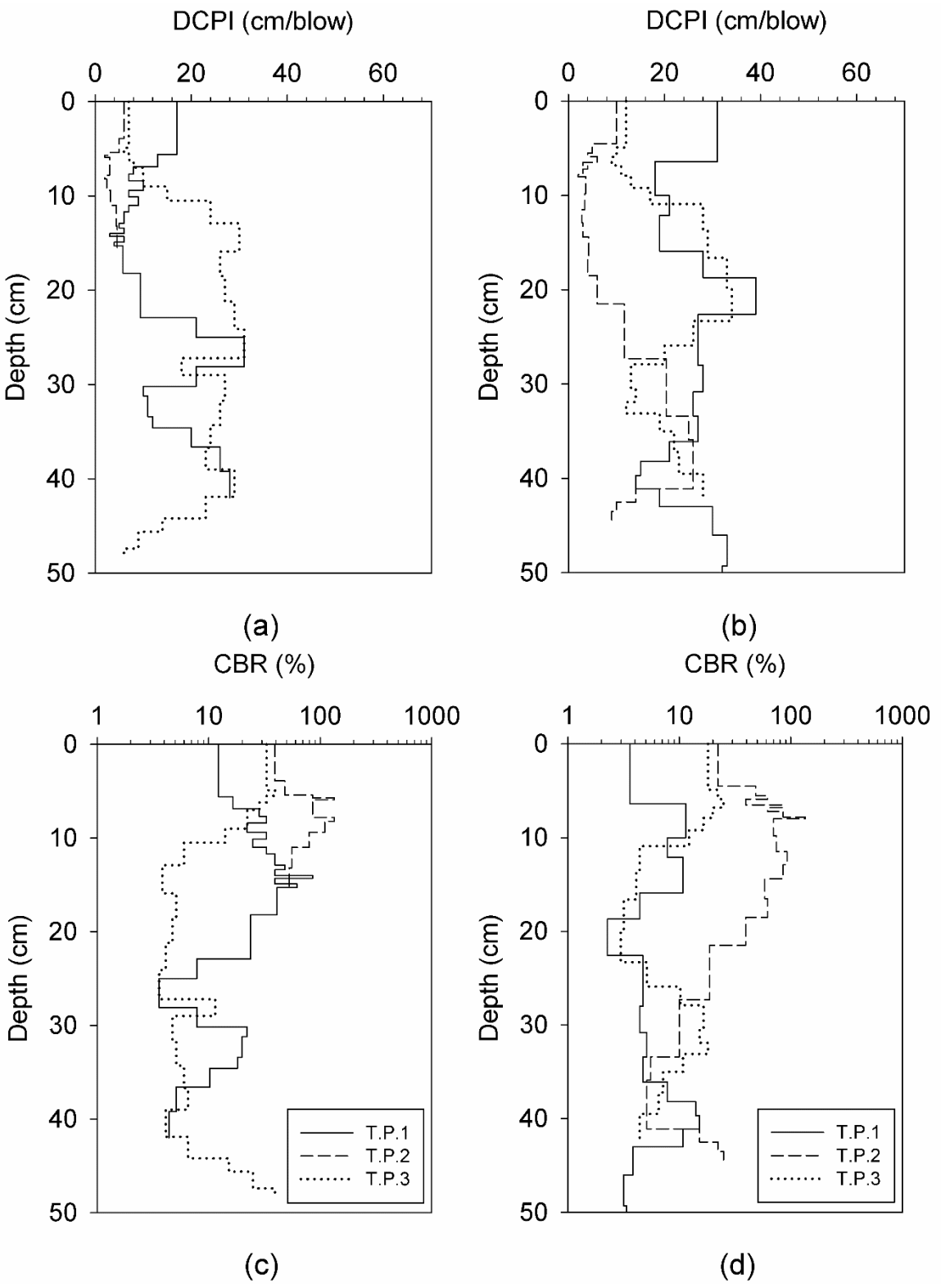


**Figure 13. DCPI and CBR results for west section of 210th Street in Boone County, Iowa, on May 22**

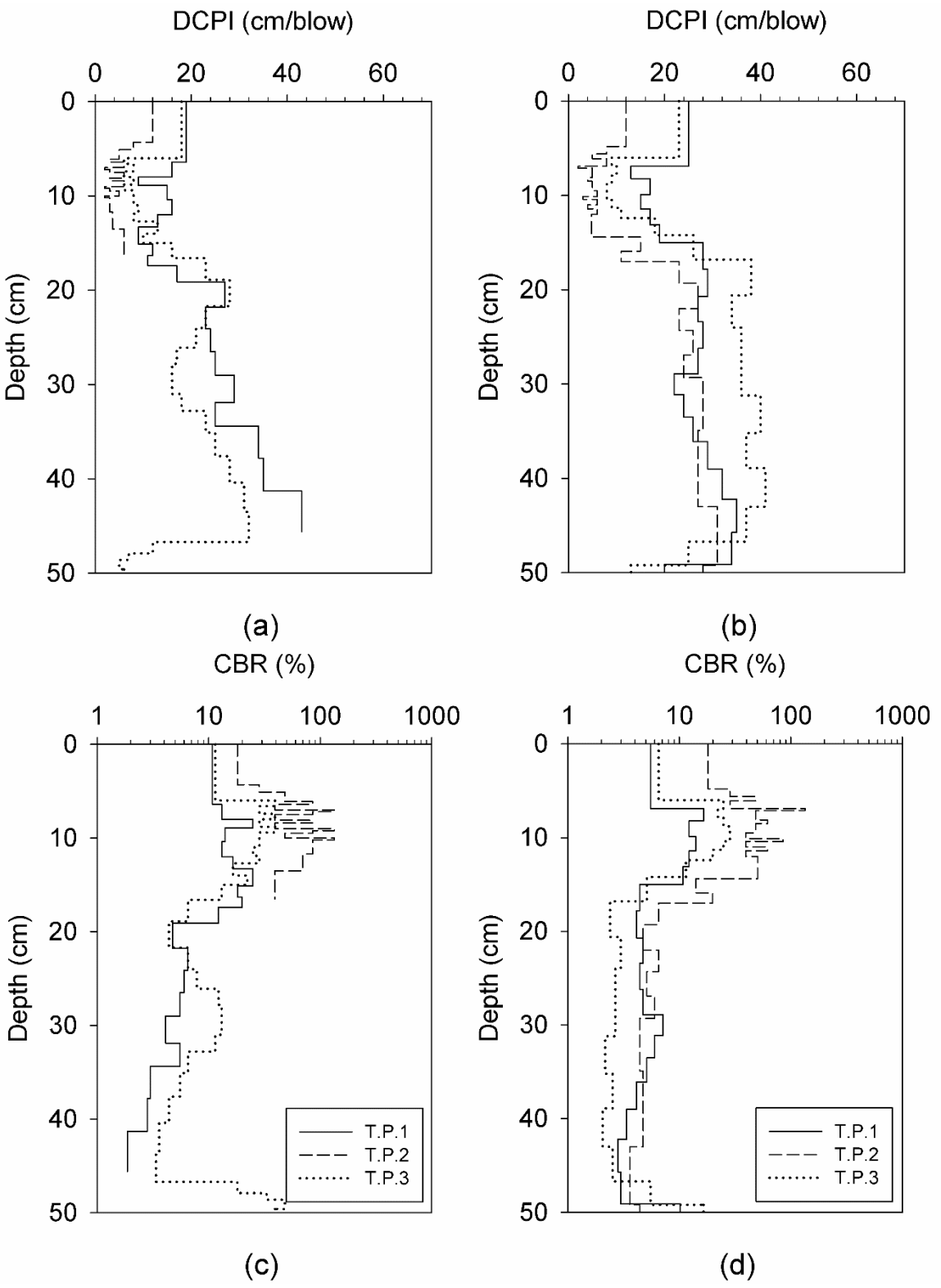


**Figure 14. DCPI and CBR results for west section of 210th Street in Boone County, Iowa, on May 25**

*East Section*

This section is located on 210th Street in Boone County, Iowa, 2,400 m (8,000 ft) east of the west section. Traffic is heavier on this section than on the west section due to vehicles from a nearby subdivision driving to X Ave. Heavy rutting occurs on this section, especially during periods of rain. County employees noted that the cross slope is shallower due to the road crown being reduced by heavy traffic. On the relatively roughest section of the roadway, small cars bottom out driving over potholes. The north side of the road was blocked off for an hour during scan days. The approximate coordinates of the laser scanner station were 42°2’57.13”N, 93°44’5.57”W. Figure 15 shows the section on different days and in different conditions.

**Figure 15. East section of 210th Street at different times: June 5 (left), June 6 (middle-left), June 8 (middle-right), and June 9 (right); blading occurred June 4 and June 15**

Figure 16 shows the gradation curve of the surface materials collected from the site on May 28. The samples were collected at two locations. It can be seen in Figure 16 that there is no evidence for a large variation in the material gradation. However further testing is needed to verify this observation.

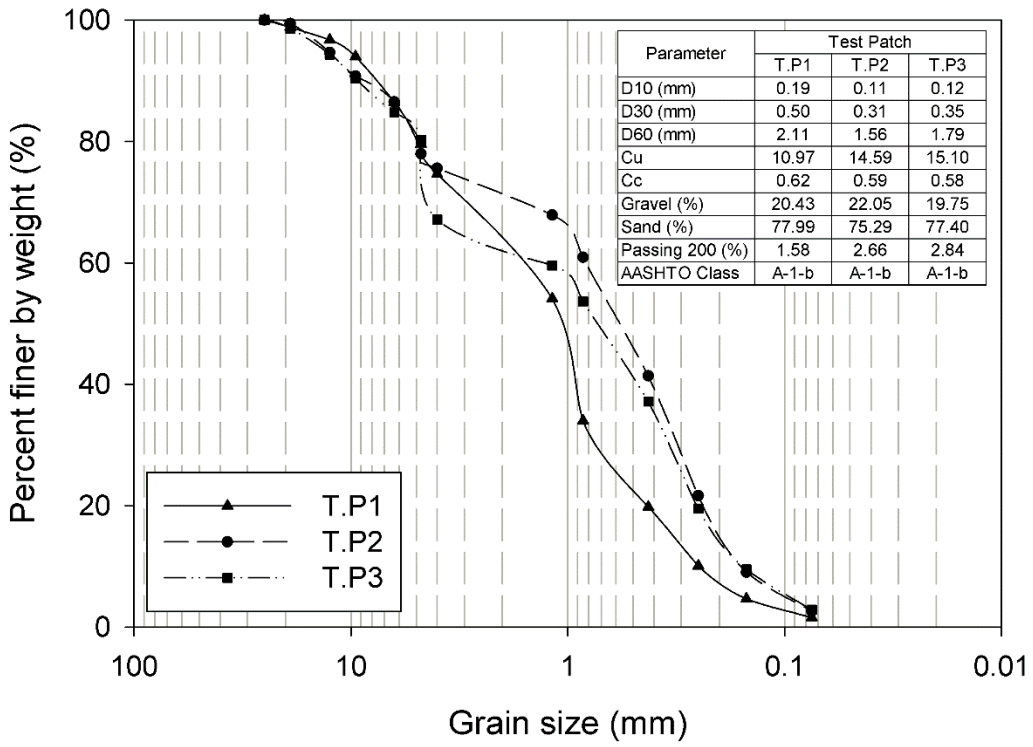


**Figure 16. Grain size distribution of surface material for east section of 210th Street in Boone County, Iowa**

Figure 17 (a) and Figure 17 (b) show DCPI versus depth for the three test points tested on June 5 in the right lane heading east and in the left lane heading west, respectively. Figure 17 (c) and Figure 17 (d) show DCP-CBR versus depth for the same three test points.

Tests were conducted to an approximate depth of 100 cm. It can be seen there are stiff laminae (DCP-CBR > 80%) down to depths of 15 cm. However, the top 5 cm are weaker, which corresponds to the loose materials at the surface.

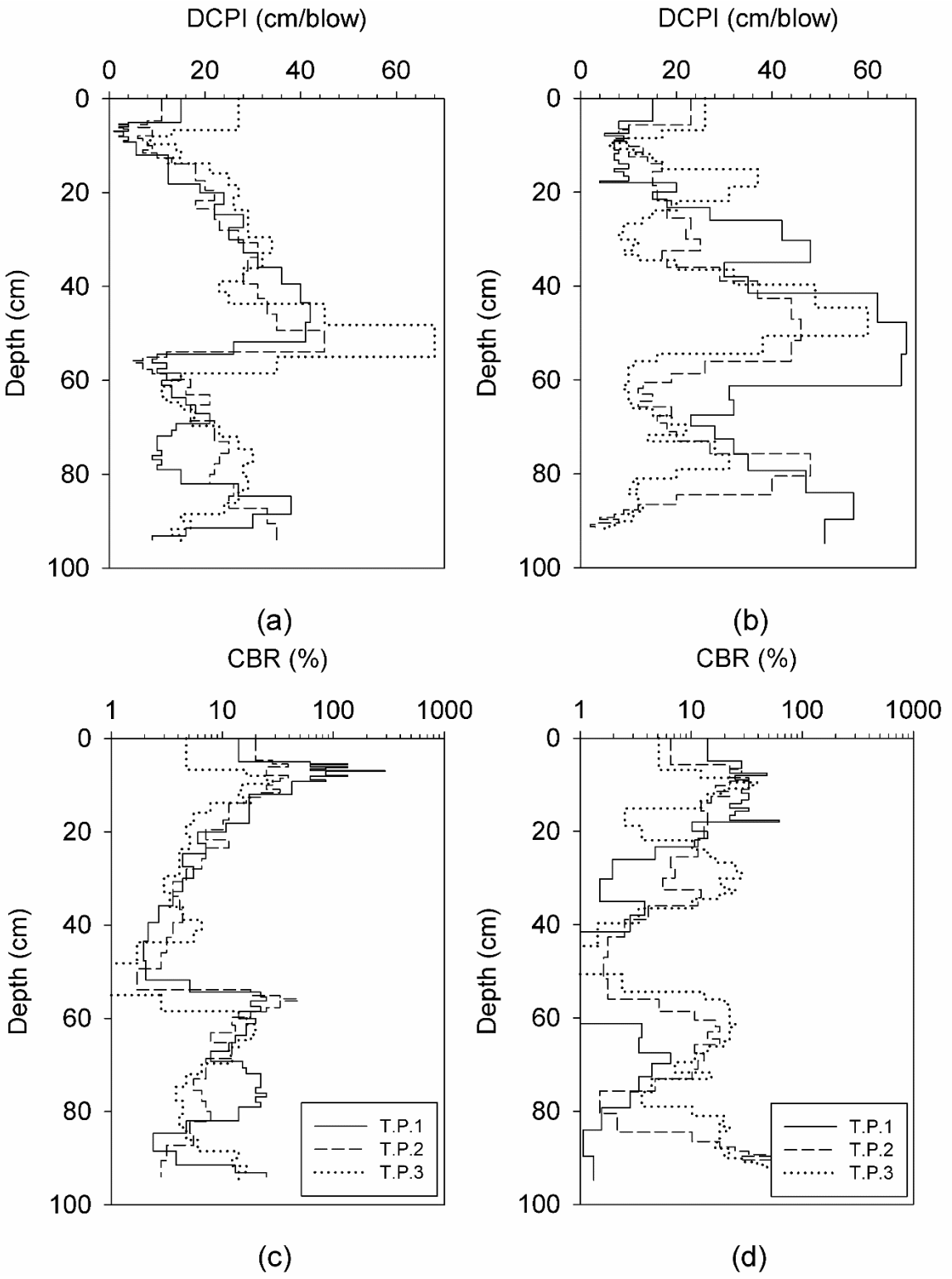


**Figure 17. DCPI and CBR results for the east section of 210th Street in Boone County, Iowa, on June 5**

**Story County Sections**

This section is located on 520th Avenue in Story County, Iowa, and is constructed of a crushed limestone aggregate surface with a treated crown. The section is located 100 m (300 ft) from an intersection, which causes vehicles to frequently slow down to turn. The west side of the road was blocked off for an hour during scan days. The approximate coordinates of the laser scanner station were 41°58’43.63”'N, 93°39’31.15”'W. Figure 18 shows the section on different days and in different conditions.

**Figure 18. 520th Avenue in Story County at different times: June 1, June 9, June 10, and June 16. Blading occurred June 9 and June 29**

A minimal amount of material was collected because of the stiff crust; the only material collected was the large aggregate on the thin top layer. DCP tests were attempted, but all tests resulted in refusals at the top. However, DCP tests were conducted on May 27 at the shoulder to depths of 100 cm. Figure 19 show DCPI versus depth for the three test points tested on May 27. It can be seen in Figure 19 that the materials are relatively soft (CBR< 80%).

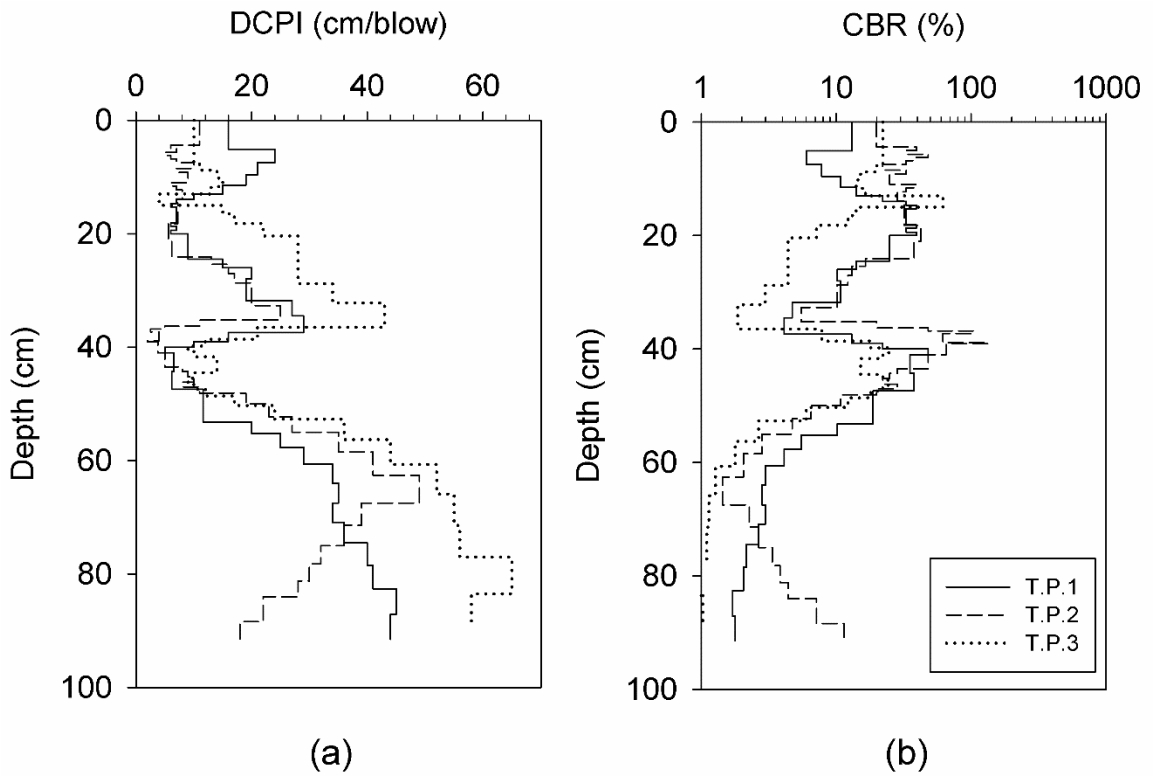


**Figure 19. DCPI and CBR results for 520th Avenue in Story County, Iowa, on May 27**

**Wilson Parking Lot**

Scans were taken before (Figure 20) and after (Figure 21) the paving of a parking lot located northwest of Wilson Hall on the Iowa State University campus. The parking lot is an asphalt overlay on a milled asphalt surface.

**Figure 20. Wilson parking lot before paving**

**Figure 21. Wilson parking lot after paving**

Due to the width of the section, three stations were set up to cover the full range. The scans acquired via TLS did not record many points due to the very low reflectivity of the fresh asphalt, and no profiles could be constructed for analysis. However, a spatial comparison of the raw point clouds produced by TLS and photogrammetry was conducted.

**South Highway 69 Concrete Section**

This section is a concrete overlay of a milled roadway surface. The concrete was placed by a slip-form paver. The approximate coordinates of the laser scanner station were 41°52’22.10”N, 93°36’1.47”W. Figure 22 shows the milled section before paving, and Figure 23 shows the section’s concrete surface after paving.

**Figure 22. Milled concrete surface of the south section of Highway 69 before paving**

**Figure 23. Concrete surface of the south section of Highway 69 after paving**

**North Highway 69 Asphalt Section**

Four scans of this section were taken. The base aggregate, chokestone, intermediate asphalt, and finished asphalt layers were captured. Monuments were also left in place for monitoring of the roadway in the future. The approximate coordinates of the laser scanner station were 41°55’6.01”N, 93°36’36.02”W. Figure 24 shows the intermediate asphalt layer, and Figure 25 shows the finished asphalt layer.

**Figure 24. Intermediate asphalt layer of the north section of Highway 69**

**Figure 25. Finished asphalt layer of the north section of Highway 69**

# CHAPTER 5: DATA ANALYSIS METHODS

After cleaning and segmenting the point clouds, the data were processed using algorithms developed to produce roughness maps. The first step in analyzing the data is to form a mesh grid from the discrete measurement points. The grid elements use predefined x and y edge dimensions to form a grid region. The grid's center elevation is calculated as the median of all cloud points falling within that grid region. All points are rotated and translated to a local coordinate system corresponding to the longitudinal and transverse axes (Alhsan et al. 2015).

A longitudinal strip is defined as a sequence of grid elements in the x direction having one y coordinate. This approach leads to a two-dimensional (2D) model where the elevation input z is a continuous function of the variable x and the fixed coordinate y. However, the discreteness of the measurements and the additional discreteness introduced by gridding the data produces a finite number of profiles that approximates the continuous 2D function. In this study, profiles with more than 40% data loss were excluded from the analysis.

Missing points (i.e., empty grids) at the beginning and end of a strip were excluded as well to avoid extrapolation. Missing points falling between two defined points were interpolated using a shape preserving piecewise cubic (Fritsch and Carlson 1980). This interpolation technique was chosen over other available techniques in MATLAB because it produces a smooth interpolation and prevents overshooting the interpolated values near the edges.

## Roughness Analysis

The evaluation of roughness in this study is based on the responses of a mechanical system that approximates the response of a passenger vehicle. The mechanical system simulated herein is the quarter-car model described in ASTM E1926-08 (2008). The quarter-car model was chosen over other models (i.e., half-car or full-car models) to define the point-wise mechanical responses of a single profile. Other models require the incorporation of two or four points on a surface to define the mechanical response for a simulated vehicle, which would change the details required to produce spatial maps of pavement roughness. Figure 26 presents a schematic of the quarter-car model.

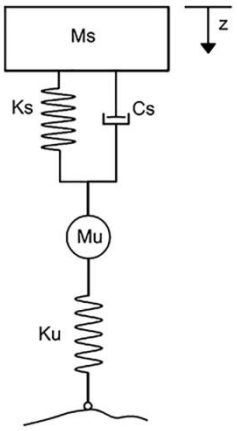


**Figure 26. Quarter-car model**

Ms and Mu are the sprung and unsprung masses, respectively; Ks and Ku are the suspension and tire spring coefficients, respectively; and Cs is the suspension damping rate. The dynamics of the system can be described by four first-order differential equations presented in matrix form (Sayers and Karamihas 1996):

$$\dot{X} = AX + B\,h_{ps} \tag{4}$$

where

$$X = \begin{bmatrix} z_s & \dot{z}_s & z_u & \dot{z}_u \end{bmatrix}^T \tag{5}$$

$$A = \begin{bmatrix} 0 & 1 & 0 & 0 \\ -k_2 & -c & k_2 & c \\ 0 & 0 & 0 & 1 \\ \frac{k_2}{\mu} & \frac{c}{\mu} & -\frac{(k_1 + k_2)}{\mu} & -\frac{c}{\mu} \end{bmatrix} \tag{6}$$

$$B = \begin{bmatrix} 0 & 0 & 0 & k_1/\mu \end{bmatrix}^T \tag{7}$$

where $h_{ps}$ is the elevation of the profile after applying the moving average smoother, $z_s$ and $z_u$ are the elevations of sprung and unsprung masses, $\dot{z}_s$and $\dot{z}_u$ are elevation time derivatives of the sprung and unsprung masses, $k_1$ is the tire spring coefficient divided by the sprung mass, $k_2$ is the suspension spring coefficient divided by the sprung mass, $c$ is the suspension damping rate divided by the sprung mass, and $\mu$ is the ratio of unsprung to sprung mass. FORTRAN code is provided in ASTM E1926-08 (2008) to solve this system. In this paper, FORTRAN code was translated to MATLAB code and used to simulate the quarter-car model over each longitudinal

strip in the grid. Because each profile is simulated independently, transverse effects such as rolling and pitch are not included.

Once the simulation is completed, roughness maps are generated for each section. The grid elements in these maps represent the rectified slope (suspension rate) of the quarter-car model at each point. This representation helps visualize and quantify the spatial distribution of roughness in a road. The lengths of the profiles are different due to the exclusion of empty grid cells at the boundaries, and thus the maps have nonuniform shapes in some cases. IRI values were also calculated to summarize the section roughness. The calculation is done by averaging the absolute rectified slope along each strip, which produces multiple IRI values across the width.

**Terrestrial Laser Scanning and Photogrammetry Comparison**

To compare the point clouds obtained from terrestrial laser scanning and photogrammetry, the coordinates of the clouds for the same section on the same date were matched in CloudCompare (Girardeau-Montaut 2015). The clouds were discretized and organized following the same approach described previously. Each longitudinal strip from the TLS grid was matched with a strip from the photogrammetry grid. Cross correlation was then calculated for these strips at lag zero to estimate the similarity between them, as described in Equation (8). The grids resulting from TLS and photogrammetry were also analyzed using a quarter-car model to produce roughness maps. The cross correlation of the strips was then analyzed in the map.

$$r_y = \frac{1}{n} \frac{\sum_{i=1}^{n} \left(t_{i,y} - \bar{t}_y\right)\left(p_{i,y} - \bar{p}_y\right)}{\sigma_{t,y}\sigma_{p,y}} \quad \textbf{(8)}$$

where $r$ is the cross correlation value calculated from n elements in a strip, subscript $y$ indicates the element of a strip with a given coordinate $y$, subscript $t$ is the elevation or suspension response of a grid element from the TLS grid, subscript $p$ is the elevation or suspension response of a grid element from the photogrammetry grid, $\bar{t}_y$ and $\bar{p}_y$ are the sample means for the strip under consideration, and $\sigma_{t,y}$ and $\sigma_{p,y}$ are the standard deviations of the elements in a strip.

## CHAPTER 6: TIME-LAPSED LASER SCANS

Following the described setup and analysis, five sections were scanned and analyzed over time. Three unpaved sections were scanned over time; the streets serve residential areas and farms with a few agricultural facilities. The scanning period began after the section was bladed, and scans were taken whenever possible. Two paved sections were scanned during construction, and scans were acquired for each layer in the construction process.

Figure 27 represents the roughness maps between May 28 and June 4 (one blading cycle) for the west station on 210th Street in Boone County, Iowa.

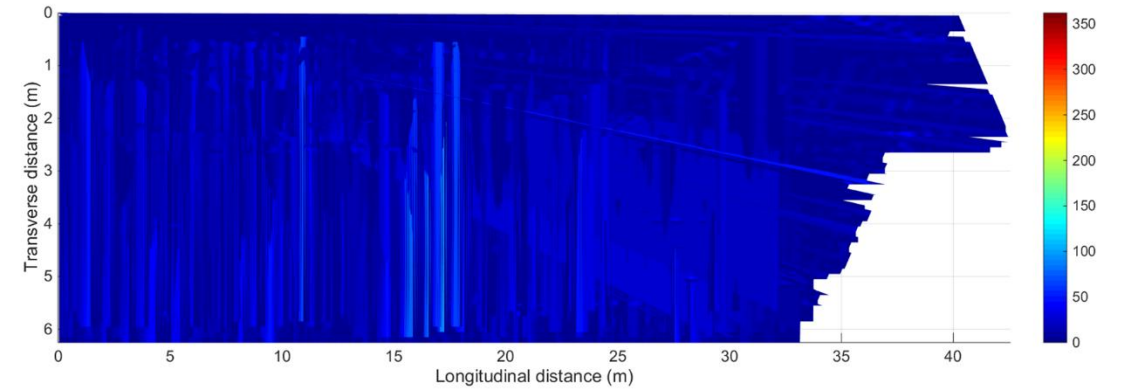
Transverse distance (m)
Longitudinal distance (m)

(a)

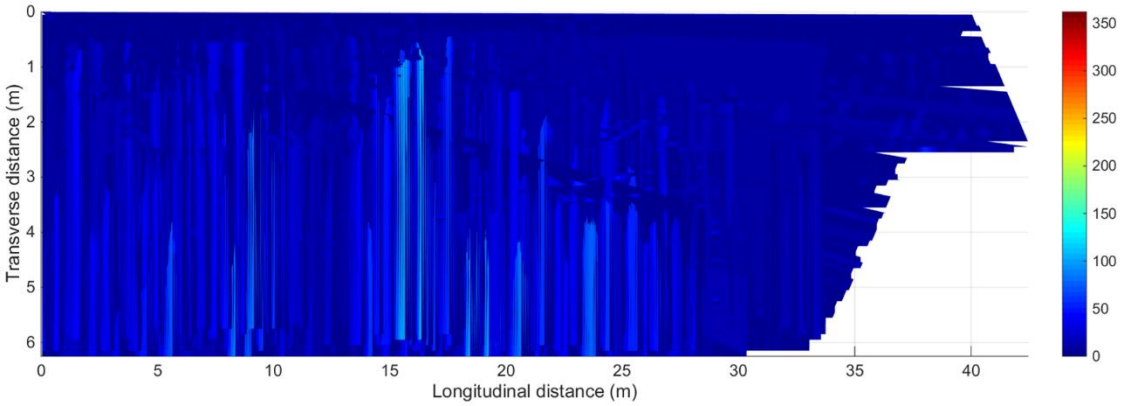
Transverse distance (m)
Longitudinal distance (m)

(b)

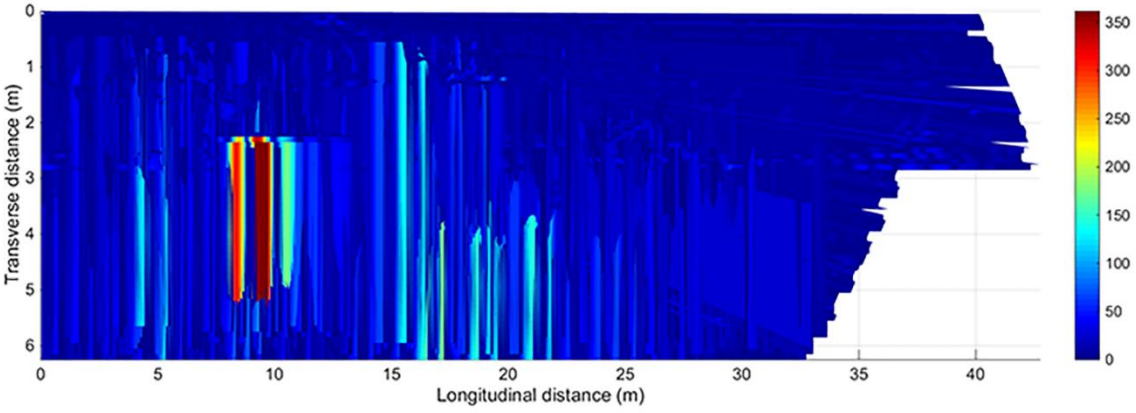
Transverse distance (m)
Longitudinal distance (m)

(c)

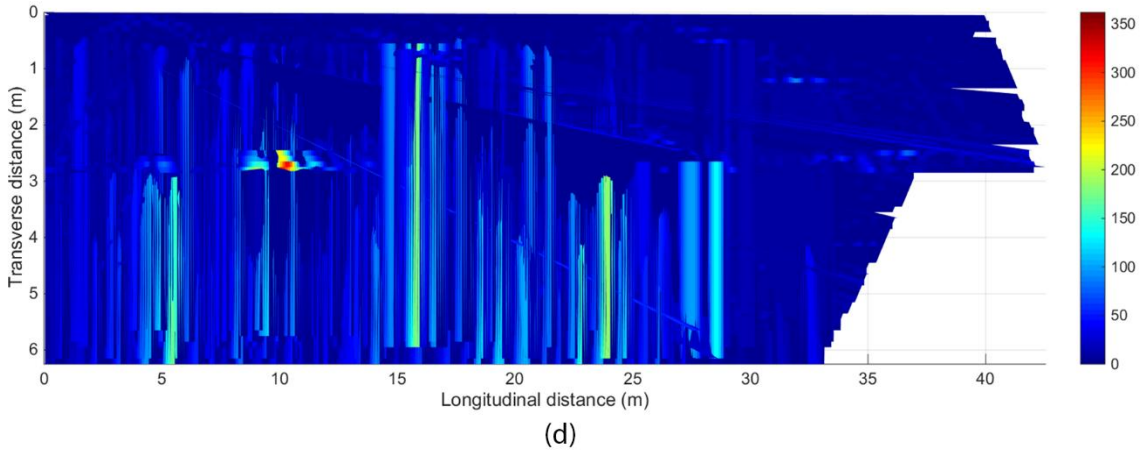


**Figure 27. Roughness maps over time for the west section of 210th Street in Boone County, Iowa: (a) May 28, (b) June 1, (c) June 3, and (d) June 4**

The color code represents the absolute value of the rectified slope in m/km, which are the same units used by IRI. It can be seen that the values vary from 0 to up to 350 m/km. However, when averaged along a strip, IRI does not reach such extreme values. It can also be seen from Figure 27 that there is a localized feature appearing around 10 m from the left edge and near the middle of the road. There is also some corrugation growing between the stations at 15 and 20 m. Overall, given the amount of data collected it is difficult to construct a statistical model that describes the dynamics of rough features on unpaved roads.

Figure 28 and Figure 29 show IRI versus width for the west and east stations on 210th Street in Boone County, Iowa.

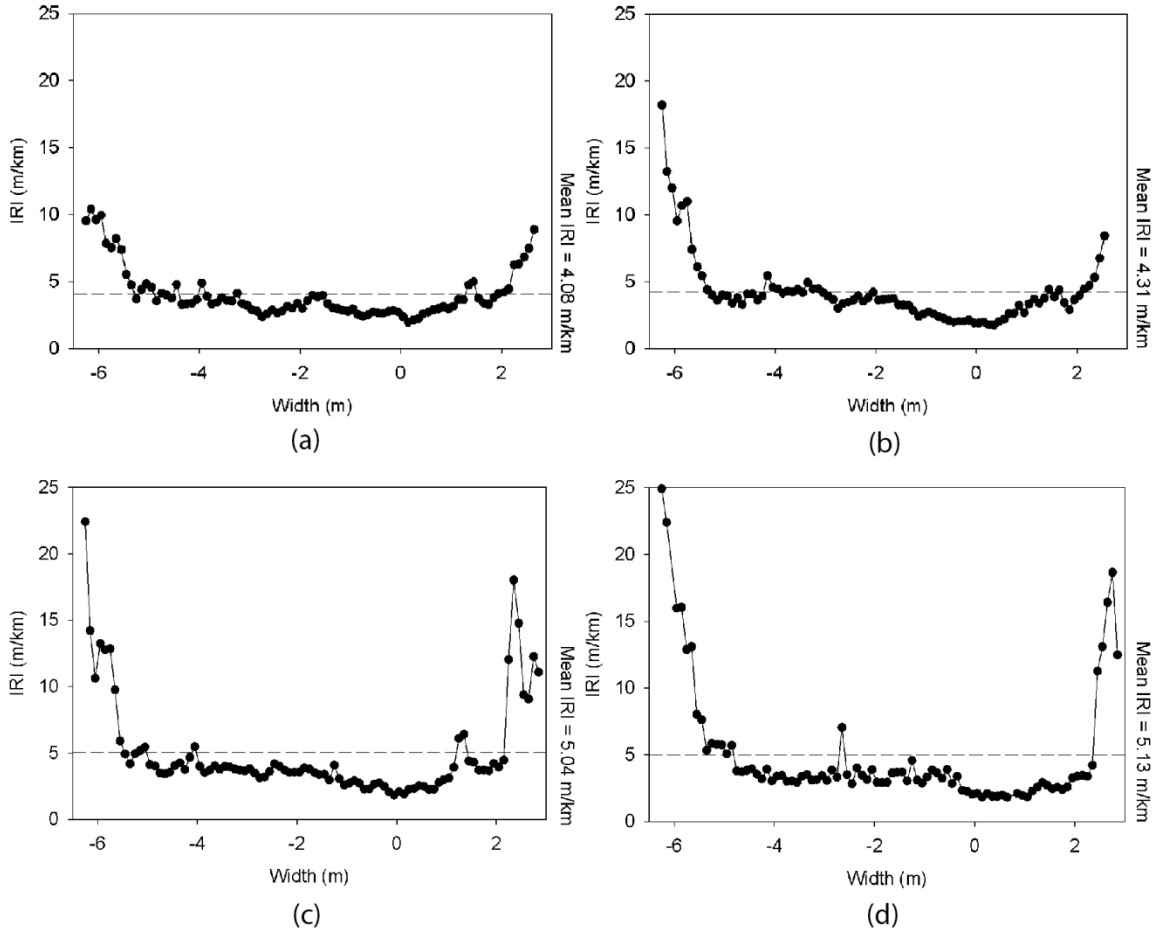


**Figure 28. IRI versus width over time for the west section of 210th Street in Boone County, Iowa: (a) May 28, (b) June 1, (c) June 3, and (d) June 4**

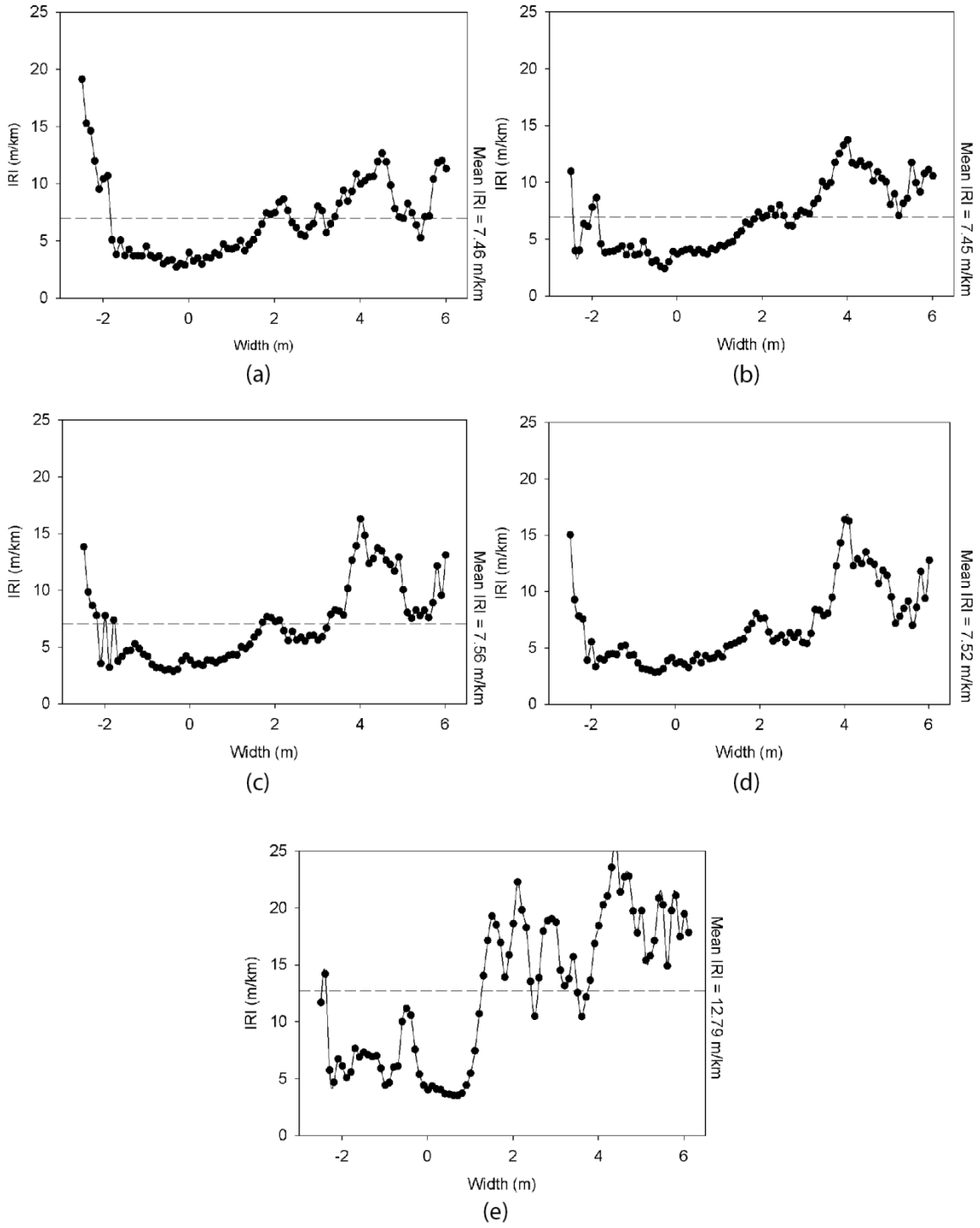


**Figure 29. IRI versus width over time for the east section of 210th Street in Boone County, Iowa: (a) June 5, (b) June 6, (c) June 8, (d) June 9, and (e) June 12**

The eastern section of 210th Street is close to a residential driveway, and thus many vehicles slow down near that turn. The x-axis represents the transverse distance across the section, and only three scans are presented for each section to ensure that the curves are clear and

distinguishable. It can be seen that overall there is no specific pattern that can be identified. However, the IRI values increase over time, and the eastern section is rougher than the western section. This is because stretches of roadway close to intersections suffer from more corrugation due to the fact that accelerating and decelerating vehicles increase the severity of corrugation (Skorseth and Selim 2000).

Figure 30 shows the roughness maps for the north section of US 69.

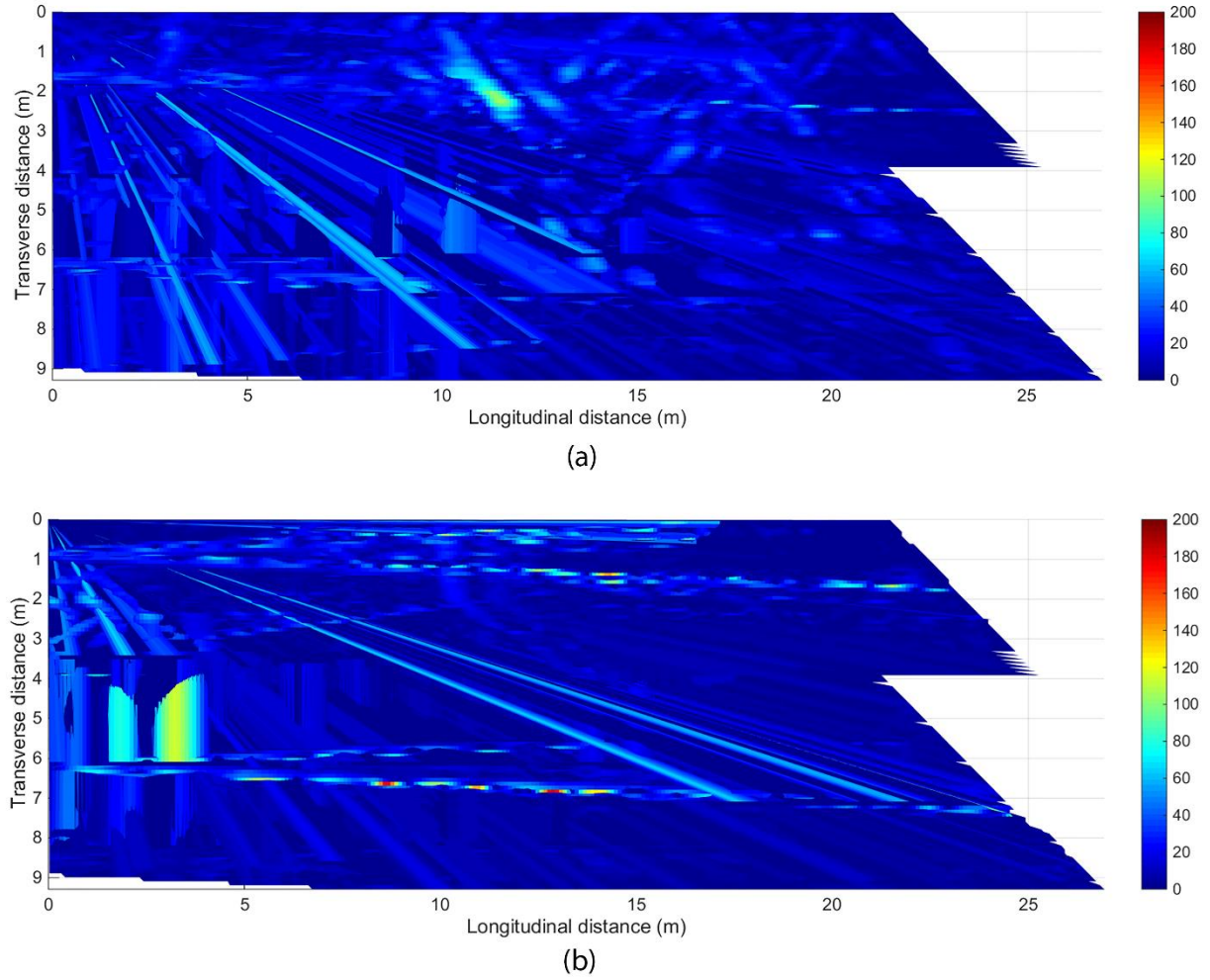


**Figure 30. Roughness maps for (a) the base layer and (b) the intermediate layer of the north section of US 69**

This is an asphalt concrete section, and the section was constructed in four layers: a base layer, a chokestone layer, an intermediate layer, and the final asphalt surface. Scans for the intermediate and final layers suffered from very high noise and are not included in the analysis. The roughness maps in Figure 30 do not show any specific patterns in this case.

Figure 31 shows the roughness maps for the south section of US 69.

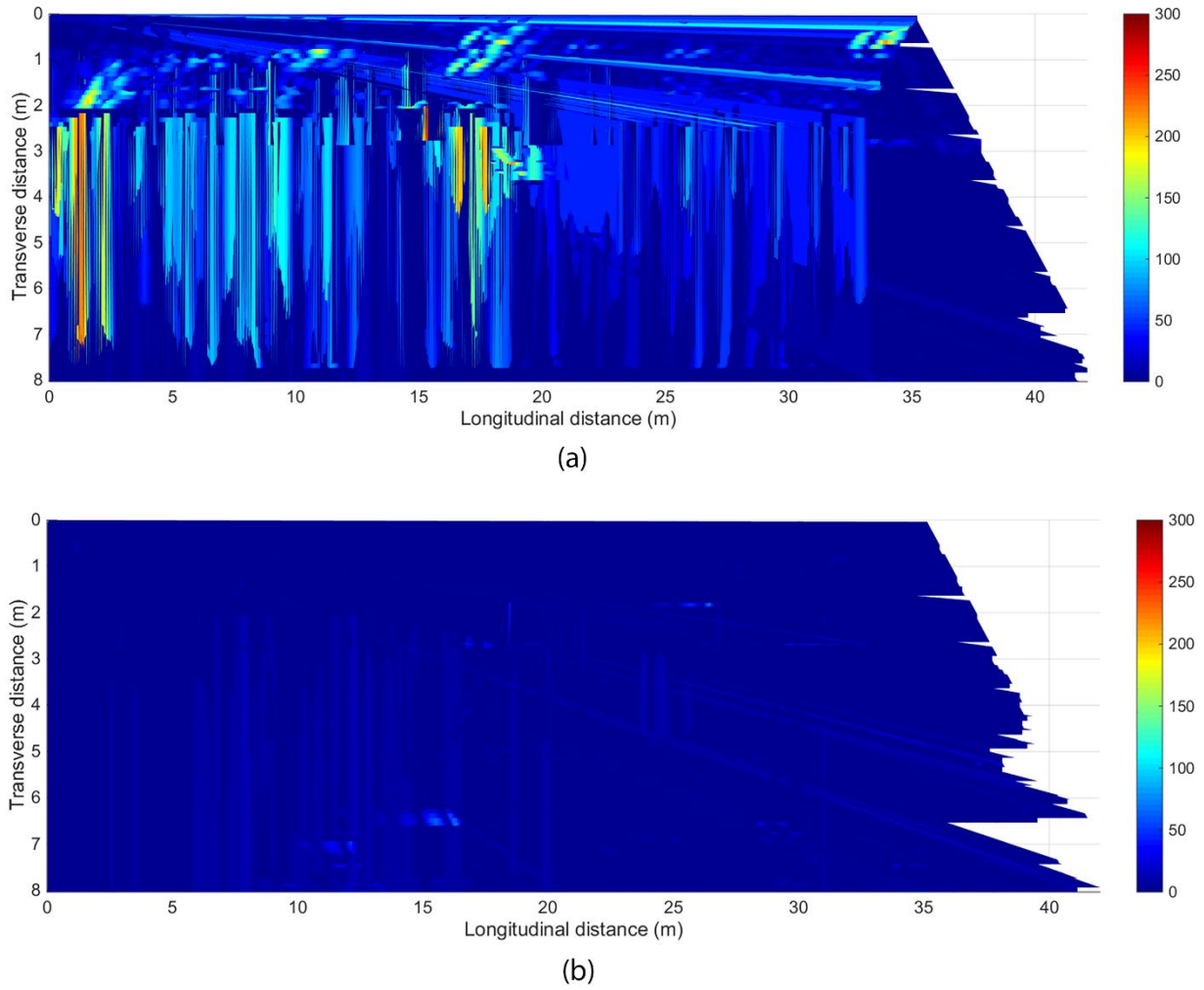


**Figure 31. Roughness maps for (a) the base layer and (b) the finished surface for the south section of US 69**

This is a PCC section. The maps in Figure 31 show the roughness of the base layer and the final surface after paving. It can be seen that there is no clear pattern in the data to confirm the correlation between the base layer and the surface layer.

## CHAPTER 7: TERRESTRIAL LASER SCANNING VERSUS PHOTOGRAMMETRY

Five point clouds were compared to evaluate TLS and photogrammetry. Two clouds (5 m long) were acquired at the west station of 210th Street in Boone County, Iowa. One cloud (15 m long) was acquired at the east station of 210th Street in Boone County, Iowa. Another cloud (34 m long) was acquired on 520th Avenue in Story County, Iowa. The fifth cloud (46 m long) was acquired on Airport Road in Ames, Iowa.

The same procedure described above was followed to discretize the point clouds and yield multiple profiles across the width. Comparisons were made using a cross correlation function for these profiles, where each profile from the TLS cloud was compared to a corresponding profile from the photogrammetry cloud. Cross correlation comparisons were made between the simulated profiles as well.

Figure 32 shows the cross correlation versus width for the elevation and suspension profiles for all tested sections.

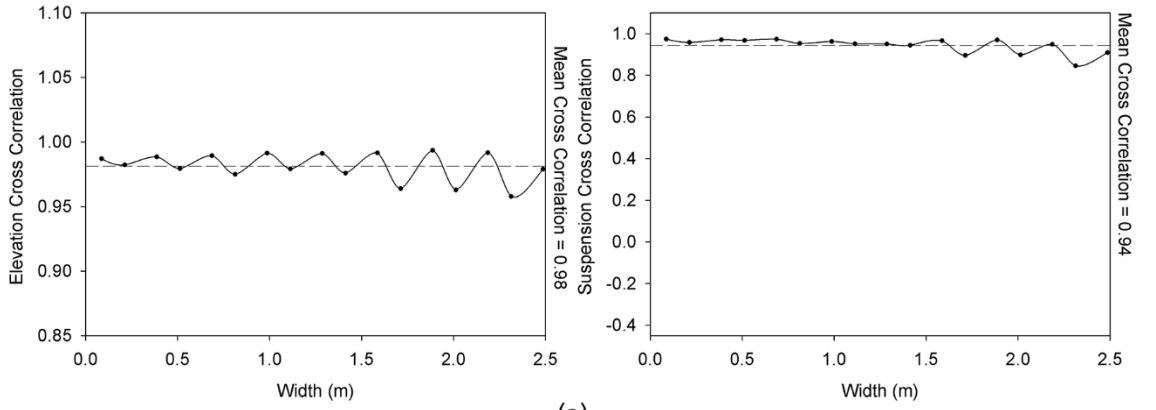
Elevation Cross Correlation
Width (m)
Mean Cross Correlation = 0.98
Suspension Cross Correlation
Width (m)
Mean Cross Correlation = 0.94

(a)

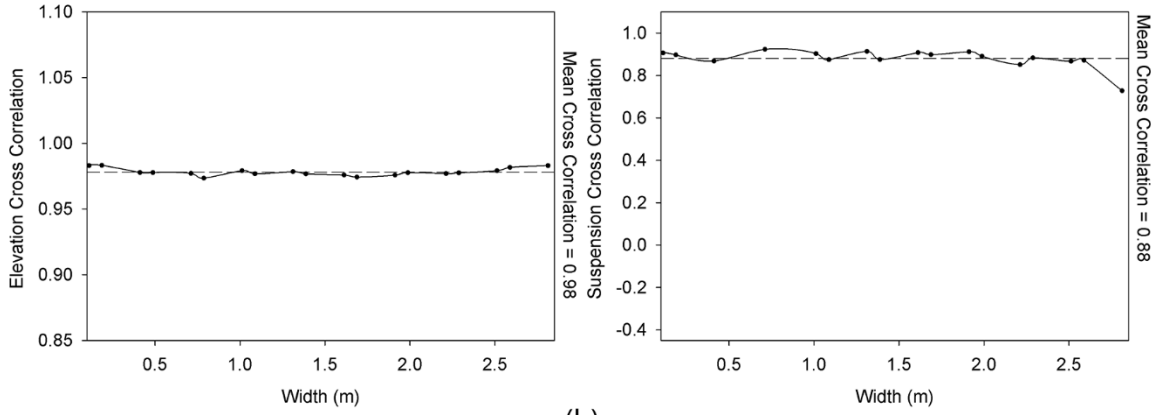
Elevation Cross Correlation
Width (m)
Mean Cross Correlation = 0.98
Suspension Cross Correlation
Width (m)
Mean Cross Correlation = 0.88

(b)

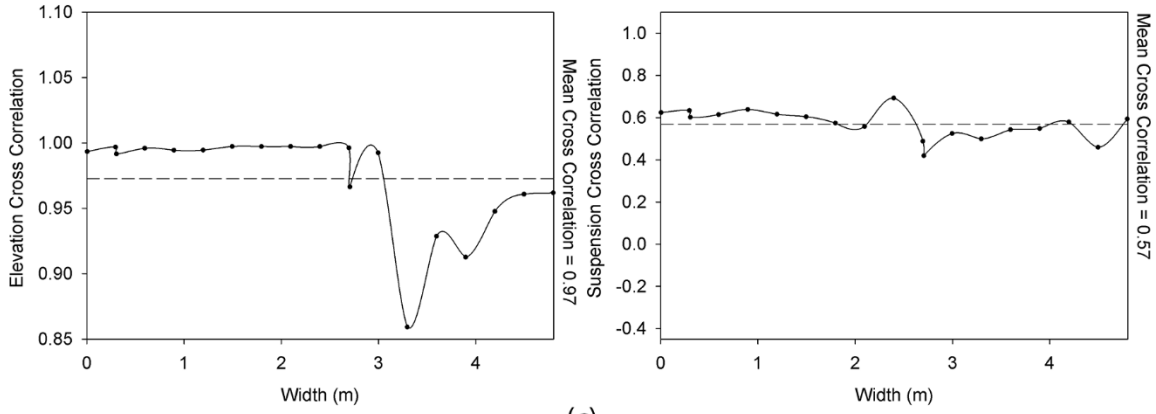
Elevation Cross Correlation
Width (m)
Mean Cross Correlation = 0.97
Suspension Cross Correlation
Width (m)
Mean Cross Correlation = 0.57

(c)

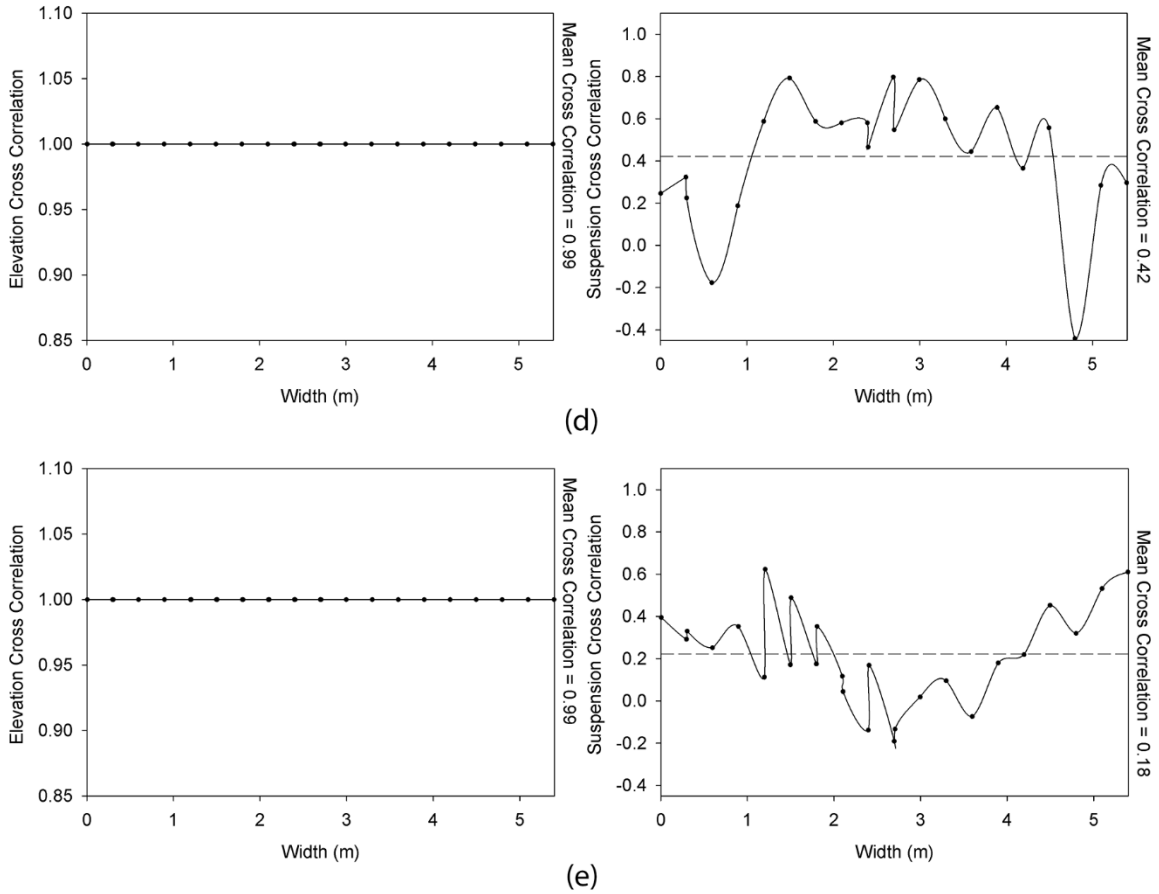


**Figure 32. Cross correlation versus width for elevation profiles (left) and suspension profiles (right) for (a) the west station of 210th Street in Boone County, Iowa (taken on June 8); (b) the west station of 210th Street in Boone County, Iowa (taken on June 9); (c) Airport Road in Ames, Iowa; (d) the east station of 210th Street in Boone County, Iowa; and (e) 520th Avenue in Story County, Iowa**

From Figure 32, it can be seen that the cross correlation for the elevation profiles is always high. However, this does not always indicate a high cross correlation between the simulated profiles. It can also be seen that the cross correlation for the simulated profiles is generally less than the cross correlation of the original profiles. However, there is a high overall correlation between the simulated profiles from photogrammetry and terrestrial laser scanning.

It should be mentioned that the profiles with low cross correlation are sampled from clouds collected on a rainy day, when the surface had many water ponds. The points around these ponds were highly scattered for both devices, though the photogrammetry clouds were more variable at these locations. Figure 33 shows the elevation profiles from the photogrammetry cloud and the TLS cloud.

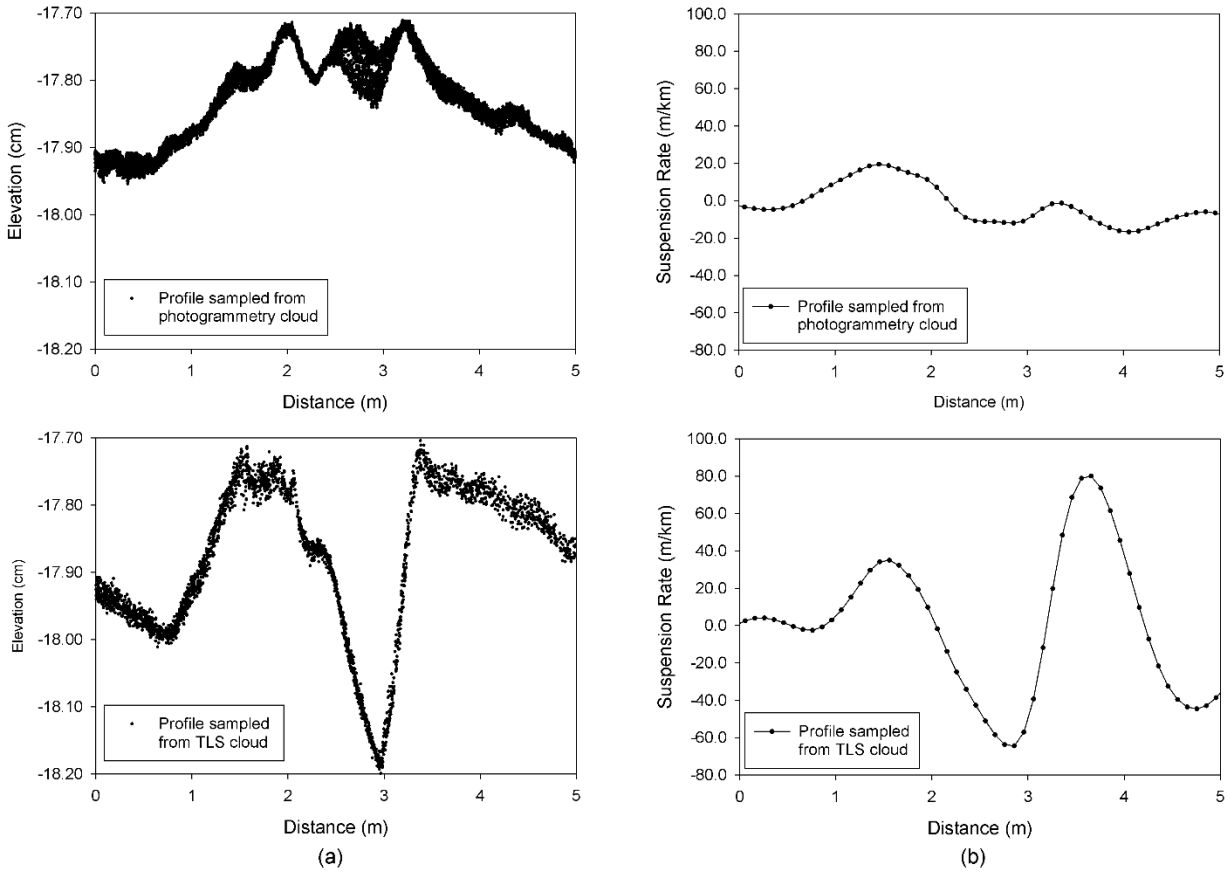


**Figure 33. (a) Elevation profiles from the photogrammetry cloud (top) and the TLS cloud (bottom) and (b) suspension profiles simulated from the photogrammetry cloud (top) and the TLS cloud (bottom)**

It can be seen in Figure 33 that the spread of the points in the profile (i.e., the variance) is high, especially at 3 m in the profile obtained from the photogrammetry cloud. This high variance led to a false conclusion of a high match (cross correlation = 0.99). However, the simulated profiles shown in Figure 31 are different, and the cross correlation between them was 0.19.

## Spatial Comparison

To analyze the spatial difference in elevation between the clouds acquired from terrestrial laser scanning and photogrammetry, the point clouds were compared directly without sampling all points. A CloudCompare plugin called Multiscale Model to Model Cloud Comparison (M3C2) was used to calculate the distances between the point clouds (Lague et al. 2013). The distances were calculated as the normal distance between two local fits in the terrestrial laser scanning cloud and the photogrammetry cloud. The maps in Figure 34 through Figure 42 show the distances between the clouds for the different roadway sections in this study.

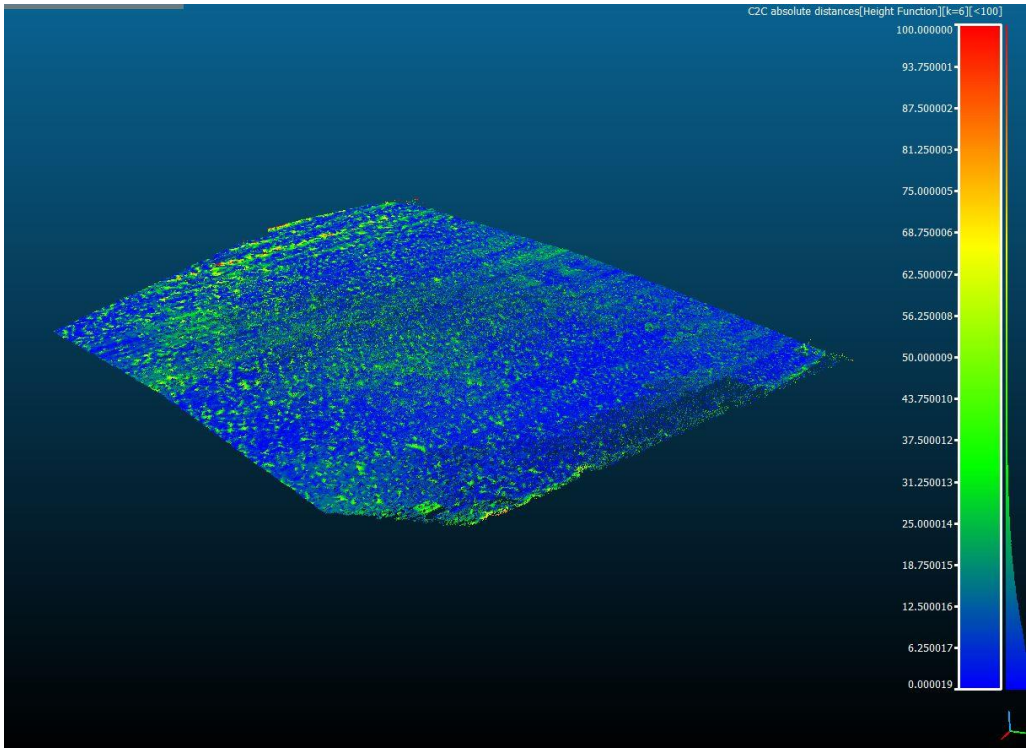


**Figure 34. Comparison of terrestrial laser scanning and photogrammetry clouds for the gravel section of 520th Avenue in Story County, June 5**

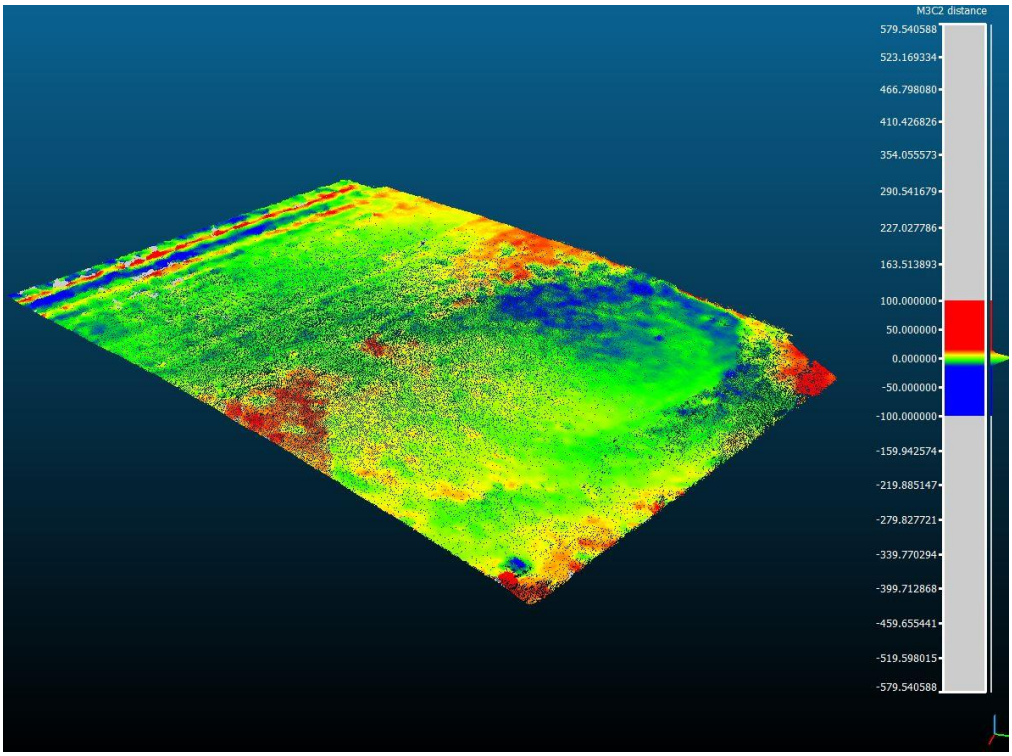


**Figure 35. Comparison of terrestrial laser scanning and photogrammetry clouds for the gravel section of 520th Avenue in Story County, June 8**

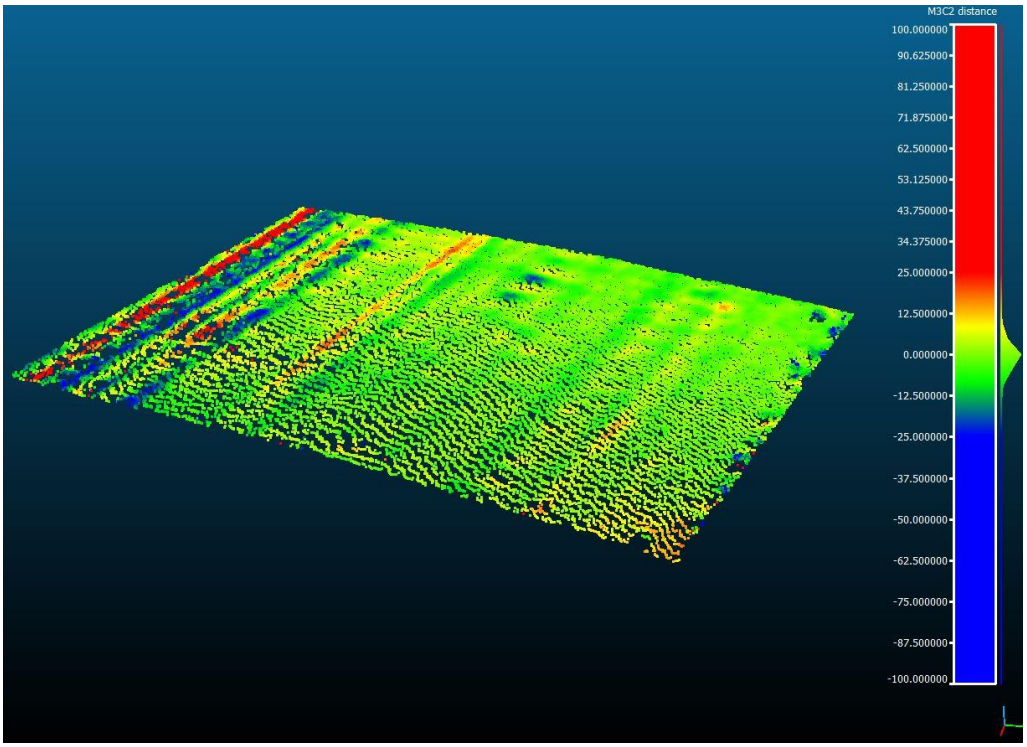


**Figure 36. Comparison of terrestrial laser scanning and photogrammetry clouds for the gravel section of 520th Avenue in Story County, June 9**

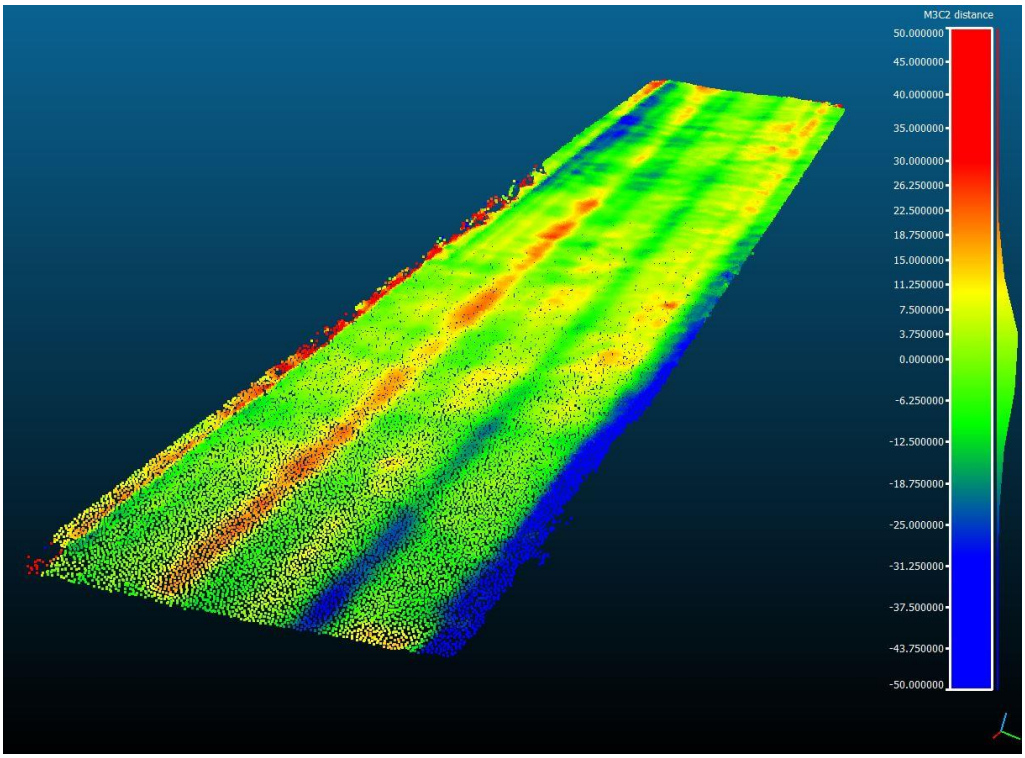


**Figure 37. Comparison of terrestrial laser scanning and photogrammetry clouds for the gravel section of 520th Avenue in Story County, June 10**

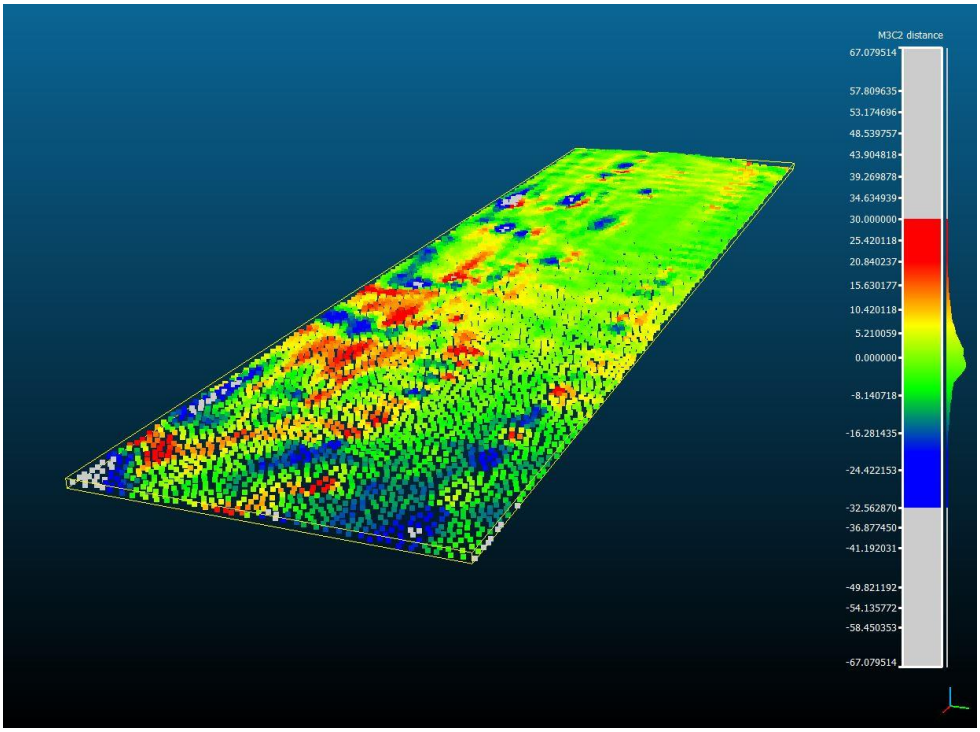


**Figure 38. Comparison of terrestrial laser scanning and photogrammetry clouds for the east gravel section of 210th Street in Boone County**

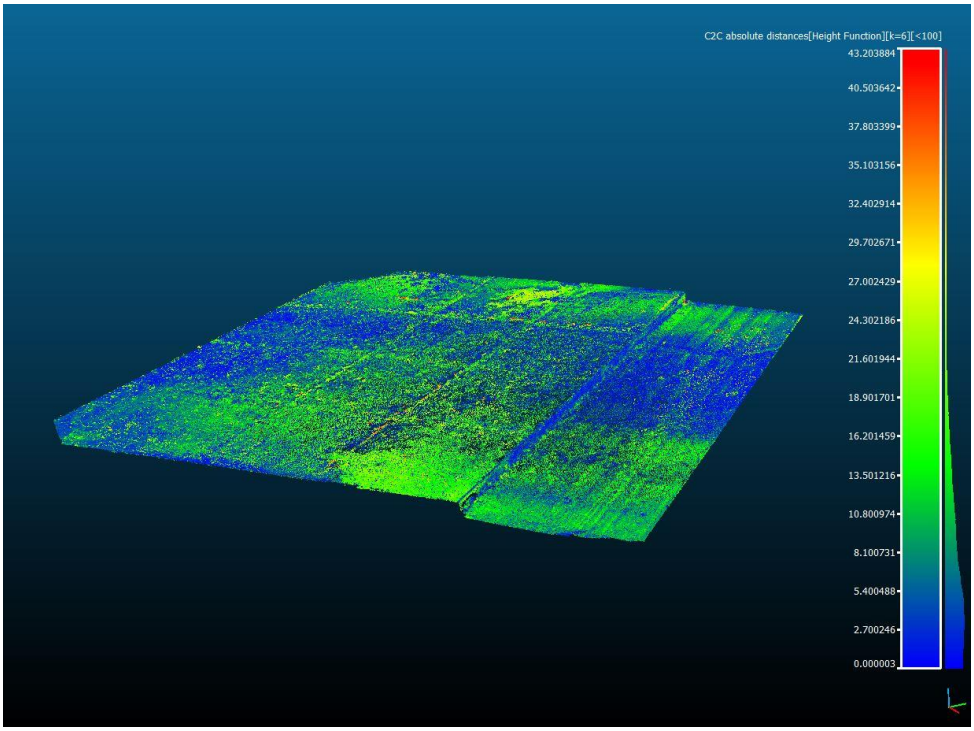


**Figure 39. Comparison of terrestrial laser scanning and photogrammetry clouds for the concrete pavement section of US 69, June 16**

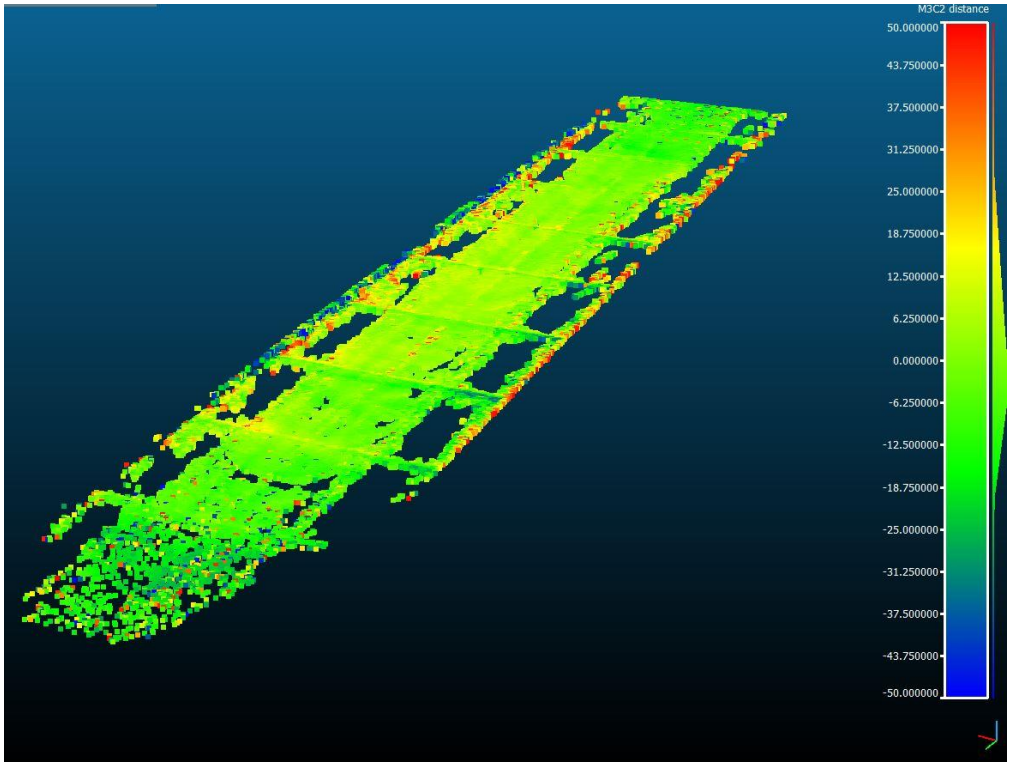


**Figure 40. Comparison of terrestrial laser scanning and photogrammetry clouds for the concrete pavement section of Airport Road in Ames, Iowa**

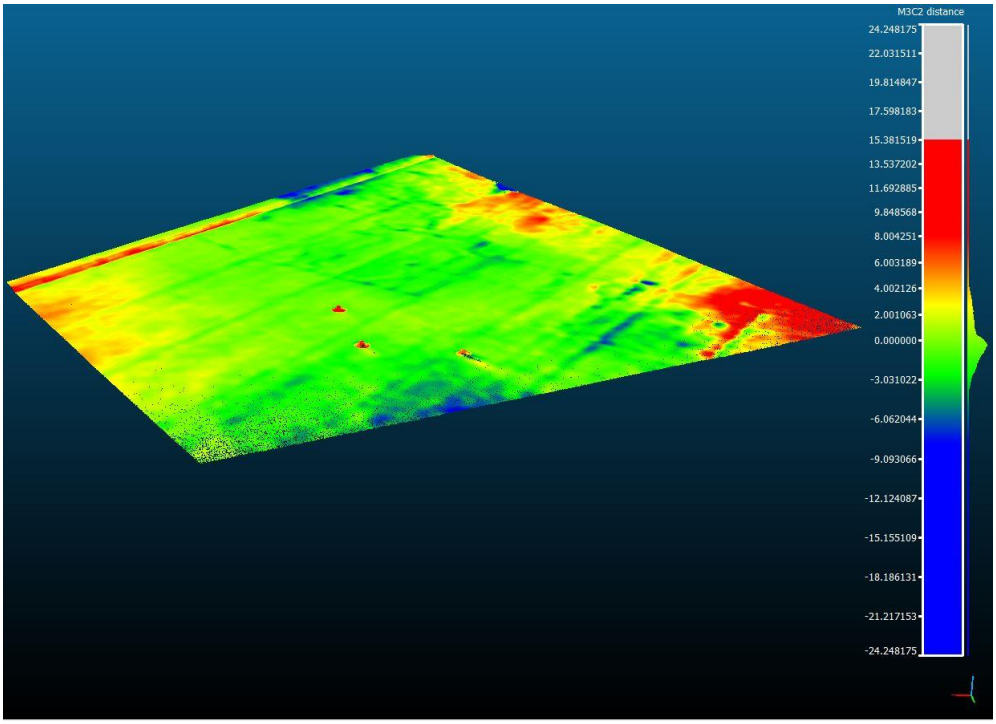


**Figure 41. Comparison of terrestrial laser scanning and photogrammetry clouds for Wilson parking lot before paving**

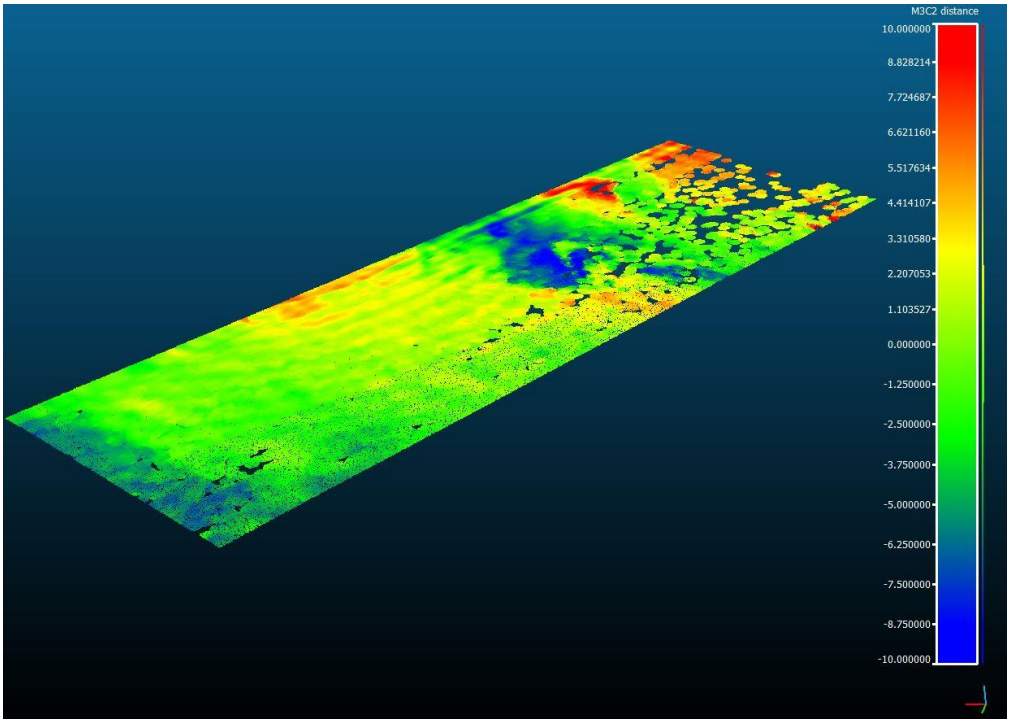


**Figure 42. Comparison of terrestrial laser scanning and photogrammetry clouds for Wilson parking lot after paving**

It can be seen in the figures that, in most cases, the greatest differences between the clouds are at rough locations. This might be due to the limitation of the laser scanner in capturing points covered by other features in the view or due to the fact that the photogrammetry algorithm produces high noise around these features due to the shadows and different lightning conditions at such features. To confirm these hypotheses, further testing is needed.

## CHAPTER 8: SOURCES OF ERROR AND LIMITATIONS

Errors can be divided to two types: bias and variance. Bias is a consistent shift in measurements, and variance is the noise in the point cloud. The variance in a point cloud collected using a given device can be evaluated by scanning a flat surface many times and evaluating the spread of the points about the surface. Bias can be tested in the same way. However, to test the bias and variance for the purposes of road roughness evaluation, the point clouds should be compared to a reliable set of ground truth data collected using a reliable setup. This ground truth testing is necessary because the acceptable level of errors depends on the application.

For terrestrial laser scanners, errors can be quantified for the equipment through calibration and can be estimated with confidence if the equipment is consistently calibrated. The variance errors are reasonability low in many cases when using a laser scanner, and the spread of the cloud is not very large. However, the bias can be high in some cases; the sources of bias are expected to be from mechanical issues in the scanner or due to a water droplet on the lens.

However, for photogrammetry-generated point clouds, the errors significantly depend on the photographer's skills, the lightning conditions, and the algorithm used in processing the photos. However, from this and previous studies it was observed that photogrammetry skills can be developed in very short period, and thus the results were improved significantly for the third point cloud collected for this project.

Another aspect to be noted is that the points obtained from the terrestrial laser scanner exhibited bias in some cases. This was suspected when matching several scans because the matched clouds had a shift near the edge, which indicated that at least one of the scans suffered from bias. On the other hand, clouds generated using photogrammetry exhibited higher variance. The cloud taken at the first roadway section studied had a very high variance, unlike the later clouds, for which the variance was reduced significantly.

External errors such as the roadway shifting due to vehicle traffic may also affect the accuracy of the comparison between photogrammetry and laser scanning. In some cases, there was up to an hour between the time when the laser scan was taken to the time when the photographs were acquired for photogrammetric reconstruction. During this time, vehicles were driving over the lanes and shifting the surface conditions. Especially in situations with a highly saturated roadway, the surface was visibly degrading whenever vehicles passed over it. In the spatial analysis of the comparison, it was observed that the driving lanes showed a slightly greater distance between the clouds than the lanes that were blocked off to traffic.

The main problem with biased clouds is that it is very difficult if not impossible to correct for the error because it is not known how much bias the system will suffer. This is especially the case if the scanner is not calibrated for a long time or some natural source of error is present, because in the field it is difficult to reanalyze the sudden conditions that cause the error. However, if a technology is proved to yield an approximately unbiased estimator and experiences well-defined variance, then specialized filters can be designed to correct for the errors and reduce the variance in the data.

High variance in the data causes very serious limitations and discrepancies in the analysis, especially because most comparisons between clouds are based on statistical inferences. For example, many software packages rely on constructing point-wise confidence intervals for one cloud and testing whether the other cloud falls within the confidence region. If so, the software indicates that the clouds are similar and that no statistical difference is suspected. However, most of these confidence intervals are derived based on parametric approaches, which in many cases require equal variances to compare the two data sets. Cross correlation can also produce false conclusions in the case of high variance in one of the sets, in that the variability in one of the sets can encompass the other cloud and thus make it appear as if the other cloud is in fact a part of the first cloud.

It was also observed in the study that TLS is not capable of acquiring points at distances exceeding 5 m for very dark surfaces with low reflectivity (i.e., fresh asphalt). However, photogrammetry could construct better point clouds in these cases. On the other hand, photogrammetry fails to produce points in some locations when the surfaces have uniform bright colors (i.e., PCC). However, TLS could acquire better point clouds in these cases.

From the study, the following limitations were identified:

- The collected data should have been compared to data from a reliable profiler to identify the level of accuracy.
- The laser scanner should have been calibrated more frequently to ensure the accuracy of the data collected.
- Given the limited project budget and timeframe, the number of tested sections was not sufficient to build firm conclusions about the roughness patterns.

## CHAPTER 9: CONCLUSIONS AND FUTURE RESEARCH

The study described in this report presented the tools to evaluate the roughness of different road types using 3D point clouds collected using two different technologies: terrestrial laser scanning and photogrammetry. The research indicates that the technologies described are very promising for evaluating road roughness. The major advantage of both technologies is the large amount of data collected, which allows the evaluation of the full road surface. Based on the analysis conducted, the following conclusions can be drawn:

- 3D laser scanning and photogrammetry techniques are powerful tools to provide detailed measurements, and with proper calibration they can be used in the analysis and characterization of pavement roughness.
- The analysis was automated, and the analysis technique can be developed further to be fully autonomous starting from the scanning stage.
- The proposed analysis technique can be used to identify localized rough features.
- Based on analysis of the results, IRI for relatively short sections is highly variable across the width of the section. This finding warrants further research.
- The proposed technique warrants additional development and verification to be standardized and used as a valuable tool for evaluating the rideability and smoothness of road surfaces.

Additional research should also include studying technologies for the automation of image collection. Images taken by unmanned aerial vehicles (UAV) for use in photogrammetry are already being widely used in agriculture, ecology, and mining applications. Applications in civil infrastructure inspection are already being explored for pavement crack detection and bridge beam deformation (Ellenberg et al. 2014). Vehicle-based camera systems for road monitoring are also potentially very useful in road inspection (Kertesz et al. 2007).

## REFERENCES


Alhsan, A., White, D. J., and De Brabanter, K. (2015), Spatial Pavement Roughness from Stationary Laser Scanning, *International Journal of Pavement Engineering* (ahead-of-print), 1-14.

Anderegg, R., and Kaufmann, K. (2004), Intelligent Compaction with Vibratory Rollers: Feedback Control Systems in Automatic Compaction and Compaction Control, *Transportation Research Record: Journal of the Transportation Research Board*, 1868(1), 124-134.

ASTM E1926-08. Standard Practice for Computing International Roughness Index of Roads from Longitudinal Profile Measurements, ASTM International, West Conshohocken, PA, 2008, www.astm.org.

Barrett, L. (2008), Automated Machine Guidance: Emerging Technology Whose Time Has Come?, pp. 5p.

Baus, R. L., and Hong, W. (2004), Development of Profiler-Based Rideability Specifications for Asphalt Pavements and Asphalt Overlays.

Bogsjö, K., and Rychlik, I. (2009), Vehicle Fatigue Damage Caused by Road Irregularities, *Fatigue & Fracture of Engineering Materials & Structures*, 32(5), 391-402.

Buchanan, J. A., Catudal, A. L., Greenshields, B. D., and Moyer, R. A. (1941), Standardizable Equipment for Evaluating Road Surface Roughness, *Highway Research Board Proceedings*, 20.

Chang, J.-R., and Chang, K.-T. (2006), Application of 3 D Laser Scanning on Measuring Pavement Roughness, *ASTM Journal of Testing and Evaluation*, 34(2), 83-91.

Chau, K., Anson, M., and Zhang, J. (2004), Four-Dimensional Visualization of Construction Scheduling and Site Utilization, *Journal of Construction Engineering and Management*, 130(4), 598-606.

Choubane, B., McNamara, R. L., and Page, G. C. (2002), Evaluation of High-Speed Profilers for Measurement of Asphalt Pavement Smoothness in Florida, *Transportation Research Record: Journal of the Transportation Research Board*, 1813(1), 62-67.

El-Korchi, T., Bacon, J., Turo, M., and Ecmecian, M. (2002), Ride Quality Assessment with Pavement Profiling Devices, *Transportation Research Record: Journal of the Transportation Research Board*, 1806(-1), 140-148.

El-Korchi, T., and Collura, J. (1998), Comparative Study of Ride Quality Measuring Devices, *Transportation Research Record: Journal of the Transportation Research Board*, 1643(-1), 125-135.

Ellenberg, A., Branco, L., Krick, A., Bartoli, I., and Kontsos, A. (2014), Use of Unmanned Aerial Vehicle for Quantitative Infrastructure Evaluation, *Journal of Infrastructure Systems*, 04014054.

Fernando, E. G., and Walker, R. S. (2013), Impact of Changes in Profile Measurement Technology on QA Testing of Pavement Smoothness: Technical Report, Texas A&M Transportation Institute.

Fernando, E. G., Walker, R. S., and Mikhail, M. (2014), Comparative Testing of Lasers for Ride Quality Measurement on HMA Pavements, *Transportation Research Board 93rd Annual Meeting*.

Fritsch, F. N., and Carlson, R. E. (1980), Monotone Piecewise Cubic Interpolation, *SIAM Journal on Numerical Analysis*, 17(2), 238-246.

Gillespie, T., Sayers, M., and Segel, L. (1980), Nchrp Report 228: Calibration of Response-Type Road Roughness Measuring Systems, *Transportation Research Board, National Research Council, Washington, DC (December 1980)*.

Gillespie, T. D., Sayers, M. W., and Hagan, M. R. (1987), Methodology for Road Roughness Profiling and Rut Depth Measurement, pp. 47p.

Girardeau-Montaut, D. (2015), Cloudcompare: 3D Point Cloud and Mesh Processing Software, *Open Source Project.*

Hannon, J. J. (2007), Emerging Technologies for Construction Delivery, Transportation Research Board, pp. 117p.

Kertesz, I., Lovas, T., and Barsi, A. (2007), Measurement of Road Roughness by Low-Cost Photogrammetric System, *International Archives of Photogrammetry, Remote Sensing and Spatial Information Sciences*, 36(5/C55), 4.

Lague, D., Brodu, N., and Leroux, J. (2013), Accurate 3d Comparison of Complex Topography with Terrestrial Laser Scanner: Application to the Rangitikei Canyon (N-Z), *ISPRS Journal of Photogrammetry and Remote Sensing*, 82, 10-26.

Nakamura, V. F. (1962), Serviceability Ratings of Highway Pavements, pp. 130p.

Oijer, F., and Edlund, S. (2004), Identification of Transient Road Obstacle Distributions and Their Impact on Vehicle Durability and Driver Comfort, *Vehicle System Dynamics*, 41, 744-753.

Perera, R., and Kohn, S. (2002), Issues in Pavement Smoothness, *Transportation Research Board, Washington, DC*.

Rasmussen, R. O., Torres, H. N., Sohaney, R. C., Karamihas, S. M., and Fick, G. (2013), Real-Time Smoothness Measurements on Portland Cement Concrete Pavements During Construction, Transportation Research Board, pp. 143p.

Sayers, M. W., Gillespie, T. D., and Paterson, W. D. O. (1986a), Guidelines for Conducting and Calibrating Road Roughness Measurements, *World Bank Technical Paper*, 87 p.

Sayers, M. W., Gillespie, T. D., and Queiroz, A. (1986b), The International Road Roughness Experiment. Establishing Correlation and a Calibration Standard for Measurements.

Sayers, M. W., and Karamihas, S. M. (1996), Interpretation of Road Roughness Profile Data.

Sayers, M. W., and Karamihas, S. M. (1998), The Little Book of Profiling, Ann Arbor: Transportation Research Institute, University of Michigan.

Skorseth, K., and Selim, A. A. (2000), Gravel Roads: Maintenance and Design Manual.

Spangler, E., and Kelly, W. (1964), Gmr Road Profilometer—a Method for Measuring Road Profile, General Motors Corporation.

Steinwolf, A., Giacomin, J., and Staszewski, W. (2002), On the Need for Bump Event Correction in Vibration Test Profiles Representing Road Excitations in Automobiles, *Proceedings of the Institution of Mechanical Engineers, Part D: Journal of Automobile Engineering*, 216(4), 279-295.

Suermann, P. C. (2009), Evaluating the Impact of Building Information Modeling (Bim) on Construction, University of Florida.

White, D. J., Vennapusa, P., and Thompson, M. J. (2007), Field Validation of Intelligent Compaction Monitoring Technology for Unbound Materials.

White, D. J., and Vennapusa, P. K. R. (2009), Report of the Workshop on Intelligent Construction for Earthworks, April 14-16, 2009, pp. 156p.